International Journal of Solids and Structures 50 (2013) 3166–3183

Contents lists available at SciVerse ScienceDirect

International Journal of Solids and Structures

journal homepage: www.elsevier.com/locate/ijsolstr

The influence of multiple cracks on tensile and compressive buckling of shear deformable beams

S. Caddemi *, I. Caliò, F. Cannizzaro

Dipartimento di Ingegneria Civile e Ambientale, Università degli Studi di Catania, Viale Andrea Doria 6, 95125 Catania, Italy

ARTICLE INFO

Article history:
Received 12 November 2012
Received in revised form 18 April 2013
Available online 7 June 2013

Keywords:
Timoshenko beam
Concentrated cracks
Buckling load
Tensile buckling
Distribution theory
Closed-form solution

ABSTRACT

In this work the static stability of the uniform Timoshenko column in presence of multiple cracks, subjected to tensile or compressive loads, is analyzed. The governing differential equations are formulated by modeling the cracks as concentrated reductions of the flexural stiffness, accomplished by the use of Dirac's delta distributions. The adopted model has allowed the derivation of the exact buckling modes and the corresponding buckling load equations of the Timoshenko multi-cracked column, as a function of four integration constant only, which are derived simply by enforcing the end boundary conditions, irrespective of the number of concentrated damage. Since shear deformability has been taken into account, the buckling load equation allows capturing both compressive and tensile buckling. The latter phenomenon has been recently investigated with reference to rubber bearing isolators, modeled as short beams, but it has been shown to occur also in slender beams characterized by high distributed shear deformation, like composite and layered beams. The influence of multiple concentrated cracks on the stability of shear deformable beams, particularly under the action of tensile loads, has never been assessed in the literature and is here addressed on the basis of an extensive parametric analysis. All the reported results have been compared with the Euler multi-cracked column in order to highlight its limits of applicability.

© 2013 Elsevier Ltd. All rights reserved.

1. Introduction

The problem concerning the analysis of damaged beams has received considerable attention in the specific literature and interesting developments have been recently proposed with regard to the adopted models, the analysis methods and the derivation of new closed-form solutions for particular structural problems.

The interest of the scientific community towards the mentioned problem is strongly motivated by the influence that damage might play in several engineering problems. To narrow down the context, the problem particularly devoted to the case of concentrated damage occurring in structural beam elements contains already different peculiarities worth of investigation. Further advanced issues concerning more complex structures are to be addressed once encouraging results are reached in the latter field.

The first studies, exploiting the theory of fracture mechanics, focussed the interest on how to model the influence of a single crack on the beam flexibility and provided expressions of the stress intensity factor for different crack geometries, different depths and different structural members (Irwin, 1957a,b; Bueckner, 1958; Westmann and Yang, 1967; Tada et al., 1985; Dimarogonas, 1996). Successive studies aimed at providing other expressions for a diffused stiffness reduction in the vicinity of the crack (Christides and Barr, 1984; Sinha et al., 2002; Chondros et al., 1998; Liebowitz et al., 1967; Liebowitz and Claus, 1968; Okamura et al., 1969). Concentrated cracks have been also modeled, according to a macroscopic approach, as an equivalent rotational spring that allows a rotation discontinuity interpreted as the crack effect on the response (Freund and Hermann, 1976; Gounaris and Dimarogonas, 1988; Rizos et al., 1990; Ostachowicz and Krawczuk, 1991; Paipetis and Dimarogonas, 1986). The previously mentioned models, based on a diffused flexural stiffness reduction, can be also approximated by adopting the equivalent spring approach whether suitable expressions for the equivalent rotational spring stiffness are introduced. The same concentrated stiffness reduction model has been adopted in the literature for the case of shear deformable beams as in Fan and Zheng (2003), Li (2001), Vadillo et al. (2012), Zapata-Medina et al. (2010), Zheng and Fan (2001b). In the latter case the model applies to slender beams composed of materials with a significant shear to Young modulus ratio, otherwise, if very short beams are considered, it is expected to apply to small depth cracks.

The effect of a single concentrated crack on the response of straight beams has been mostly evaluated under the hypothesis that the crack do not undergo the closing phenomenon (non-propagating crack), i.e. it remains open during the loading process,

* Corresponding author. Tel.: +39 0957382266; fax: +39 0957382297.
E-mail address: scaddemi@dica.unict.it (S. Caddemi).

0020-7683/$ - see front matter © 2013 Elsevier Ltd. All rights reserved.
http://dx.doi.org/10.1016/j.ijsolstr.2013.05.023

implying a linear behavior. However, abrupt (switching crack) (Zastrau, 1985; Chu and Shen, 1992; Shen and Chu 1992; Quian et al. 1990; Ibrahim et al. 1990; Caddemi et al., 2010) as well as progressive closure of the crack (breathing crack) (Cheng et al., 1999; Pugno et al., 2000; Patel and Darpe, 2008) has been accounted for in the literature.

Particularly, when damage occurrence along the beam span is not restricted to a single crack appearance, the equivalent spring approach shows to be suitable for determining competitive procedures and even closed form solutions.

In the latter case, concerning the presence of several cracks, the traditional methods, relying on the introduction of additional variables at the cracked cross-sections and subsequent enforcement of the continuity conditions, should be avoided since computationally cumbersome in the case of numerous cracks and, more importantly, do not lead to closed form solutions.

In fact, for the case of an arbitrary number of cracks different innovative approaches have been proposed. Far from being exhaustive, they can be roughly classified based on the basic idea to reduce the computational effort involved in the calculation: (i) the smooth function method (Shifrin and Ruotolo, 1999; Ruotolo and Surace, 2004); (ii) the modified Fourier series method (Zheng and Fan, 2001a); (iii) the transfer matrix method (Khiem and Lien, 2001; Li, 2002; Sorrentino et al., 2007) (iv) the distributional approach (Yavari and Sarkani, 2001; Yavari et al., 2000, 2001a, 2001b; Falsone, 2002; Wang and Quiao, 2007; Buda and Caddemi, 2007; Caddemi and Caliò, 2008, 2009, 2012; Caddemi et al., 2013).

Among the engineering problems involving straight beams, particularly important is the loss of stability of the equilibrium configuration due to buckling caused by axial loads in columns under different boundary conditions. It has been widely proved that the presence of concentrated cracks can cause a considerable decrement of the buckling loads as well as modification of the relevant buckling modes. The stability of single and multiple cracked columns has been studied both for the Euler–Bernoulli (Anifantis and Dimarogonas, 1983; Wang, 2004; Wang et al., 2004; Li, 2001; Gurel 2007) and the Timoshenko (Takahashi, 1999; Li, 2002; Zheng and Fan, 2001b; Fan and Zheng, 2003) models, with the particular purpose, in the latter case, of assessing the influence of the shear deformability of the column. To the authors' knowledge, all the studies, focussed on the buckling of cracked columns, consider the action of compressive loads, except that reported in Zapata-Medina et al. (2010) where the buckling behavior of a single cracked shear deformable column has been captured by means of a classical approach in presence also of a tensile load.

With regard to the case of compressive loads one can argue that concentrated cracks might be closed. Rigourously a breathing crack model, whose amplitude is associated to the beam curvature, should govern the transition between the closed and fully open conditions. However, in almost all the approaches considered in the literature the switching crack model is considered, according to which the crack is fully open or closed. According to the latter model, once instability occurs, the crack effect surely appears if it affects both sides of the beam (bilateral crack). On the other hand, unilateral cracks activate or not in accordance to the buckling shape curvature. Details of the latter behavior concerning buckling under compressive loads are proposed in (Challamel and Xiang, 2010).

On the other hand, the buckling phenomenon due to the action of tensile loads has been first evidenced by Kelly (2003) as occurring in rubber bearing isolators, which are characterized by high shear deformations. The tensile buckling appears, as a consequence of the significant influence of the shear deformation, in an antisymmetric shape as a result of the rotation restraints of both end of the isolator. In particular the latter phenomenon might cause unexpected local instabilities in isolated structures in some areas of the foundation where tensile loads occur.

Successively the tensile buckling has been shown to occur also in slender beams (Aristizabal-Ochoa, 2005, 2007) and, moreover, that the tensile buckling loads are not necessarily the mirror images of the compression counterparts. More recently, Zaccaria et al. (2011) showed both theoretical and experimental evidence of the tensile buckling in Euler beams in presence of shear internal discontinuities. In any case, the influence of shear deformation plays a fundamental role, since the tensile buckling load can decrease significantly and be comparable to the compressive buckling.

Furthermore, one might bear in mind that shear deformability has to be considered in those cases, such as fiber reinforced plastic composite materials and layered or functionally graded columns, showing low shear modulus.

The contribution of the present work is intended towards the formulation of closed form solutions for buckling modes and buckling load equations of shear deformable columns, affected by an arbitrary number of cracks, able to capture also the buckling phenomenon under the action of tensile loads.

The need for closed form solutions in engineering problems consists in their use for preliminary design, for evaluating the role played by various geometric and loading parameters and also providing benchmark solutions to test results provided by approximated numerical methods and discretised approaches. In particular, in the context of the buckling problem, this is confirmed in the literature by stability books (Wang et al., 2005; Elishakoff, 2005) and by the formulation of closed form solutions for inhomogeneous beams (Calio and Elishakoff, 2002, 2004a,b, 2005).

So far, the authors have studied extensively the Euler-Bernoulli beam within different contexts in presence of an arbitrary number of cracks, providing closed form solutions (Caddemi and Caliò, 2008, 2009, 2012) extended to the case of frame structures (Caddemi and Caliò, 2013a, b). The latter studies provided encouraging results based on the adoption of generalized functions (distributions) to model both flexural and shear stiffness reductions due to different causes (Biondi and Caddemi, 2005, 2007; Caddemi et al., 2013).

Aim of this paper is applying the distributional model to shear deformable columns with multiple cracks for the evaluation of the exact solution and investigation of the influence of concentrated damage distributions on tensile and compressive buckling. The adopted integration procedure leads to explicit closed-form solutions for the buckling modes and the corresponding buckling load equations of the Timoshenko column. The exact solution is a function of four integration constants only, as for the undamaged column, this analytical structure of the solution allows the derivation of the exact solution of any multi-cracked Timoshenko column simply by enforcing the end boundary conditions. A further novelty of the presented closed-form solutions is represented by the formulation of the tensile buckling of beams in presence of multiple cracks. In particular, positive roots of the buckling load equation provide compressive buckling loads, while negative roots represent the mentioned tensile buckling loads. The results are validated with those available in the literature for the case of a single crack. Then, novel results on multi-cracked columns are presented by means of an extensive parametric analysis on simply supported and clamped–clamped columns to assess the effect of an increasing number of cracks by accounting for the influence of the shear deformation.

This study, rather than design or identification purposes, contributes to the assessment of the residual carrying capacity of damaged beams, by accounting for the buckling phenomenon, once the damaged configuration of the beam if fully known.

2. A flexural stiffness model of the Timoshenko beam with multiple cracks

In this section a model of Timoshenko beam showing multiple discontinuities in the rotation function is presented, and its capability of describing the influence of concentrated cracks is shown.

The well known static governing equations of Timoshenko beams with variable flexural stiffness $E(x)I(x)$ and shear stiffness $G(x)A(x)$ in presence of an axial load N can be written, with respect to the spatial abscissa x spanning from 0 to the beam length L, as follows:

$$\frac{d}{dx}V(x)=0;\quad \frac{d}{dx}M(x)=V(x)+N\frac{d}{dx}v(x)\quad \text{Equilibrium equations} \tag{1a, b}$$

$$\chi(x)=\frac{M(x)}{E(x)I(x)},\quad \gamma(x)=\frac{T(x)}{G(x)A(x)}\quad \text{Constitutive equations} \tag{1c, d}$$

$$\chi(x)=\frac{d}{dx}\varphi(x);\quad \gamma(x)=\frac{d}{dx}v(x)+\varphi(x)\quad \text{Compatibility equations} \tag{1e, f}$$

where $V(x)$ is the vertical force while $T(x)$ and $M(x)$ are the shear force and the bending moment, respectively, $v(x)$, $\varphi(x)$ are the deflection and the rotation functions, respectively, and $\gamma(x), \chi(x)$ are the shear deformation and the curvature functions, respectively.

According to a model able to account for the shear deformability of the beam (Timoshenko and Gere, 1961) the relationship between the vertical force $V(x)$ and the shear force $T(x)$ can be inferred by considering the shear force $T(x)$ proportional to the rotation $\varphi(x)$ as follows:

$$T(x)=V(x)-N\varphi(x)\Rightarrow V(x)=G(x)A(x)\left[\frac{d}{dx}v(x)+\varphi(x)\right]+N\varphi(x) \tag{2}$$

Eq. (1), in view of the model given by Eq. (2), can be combined to provide the following differential governing equations

$$\frac{d}{dx}\left[E(x)I(x)\frac{d}{dx}\varphi(x)\right]=G(x)A(x)\left[\frac{d}{dx}v(x)+\varphi(x)\right]+N\varphi(x)+N\frac{d}{dx}v(x) \tag{3a}$$

$$\frac{d}{dx}\left[G(x)A(x)\left[\frac{d}{dx}v(x)+\varphi(x)\right]\right]+N\frac{d}{dx}\varphi(x)=0 \tag{3b}$$

Multiple singularities in the rotation functions, due to the presence of internal rotational springs at $x_{\gamma_i}, = 1,\dots,n_\gamma$, can be modeled as reductions of the reference flexural stiffness by means of the adoption of the well known Dirac's delta $\delta(x)$ distribution, as follows (Biondi and Caddemi, 2005,2007):

$$E(x)I(x)=E_0I_0D(x)\left[1-\sum_{i=1}^{n_\gamma}\overline{\gamma}_i\delta(x-x_{\gamma_i})\right] \tag{4a}$$

$$G(x)A(x)=G_0A_0H(x) \tag{4b}$$

in which $D(x)$ and $H(x)$ are dimensionless functions responsible of along-axis, both continuous and discontinuous, variations of the flexural and shear stiffnesses with respect to the values E_0I_0 and G_0A_0; furthermore, $\overline{\gamma}_i$ are parameters associated to the concentrated rotational singularities.

The stiffness reduction introduced in the model adopted in Eq. (4) can be considered equivalent to the effect produced by concentrated cracks if a suitable correspondence with the crack depth is adopted (Caddemi and Caliò, 2008, 2009). For convenience, the equivalence between the adopted model and the real crack depth is reported in the Appendix. The distributional model here adopted for concentrated cracks has been recently validated, both from a theoretical and experimental point of view, as discussed in Caddemi and Morassi (2013).

In this work the influence of concentrated cracks on the shear stiffness is neglected hence no deflection discontinuities are accounted for. Furthermore, the suitability of the concentrated crack model when the shear deformation effect plays a significant role in the response behavior is addressed in the numerical application section.

For simplicity, by considering the dimensionless coordinate $\xi=x/L$, and indicating with the apex the differentiation with respect to ξ, the governing differential equations of the Timoshenko beam given by Eq. (3), by accounting for the singularities introduced in Eq. (4), take the following form:

$$\left[D(\xi)\left[1-\sum_{i=1}^{n_\gamma}\gamma_i\delta(\xi-\xi_{\gamma_i})\right]\varphi^I(\xi)\right]^I = br^2H(\xi)\left[u^I(\xi)+\varphi(\xi)\right]+\sigma^2\left[u^I(\xi)+\varphi(\xi)\right] \tag{5}$$

$$br^2\left[H(\xi)\left[u^I(\xi)+\varphi(\xi)\right]\right]^I+\sigma^2\varphi^I(\xi)=0 \tag{6}$$

In Eqs. (5) and (6), the normalized function $u(\xi)=\frac{v(\xi)}{L}$ and the normalized axial load $\sigma^2=\frac{NL^2}{E_0I_0}$ have been introduced and the property $\delta[L(\xi-\xi_i)]=(1/L)\delta(\xi-\xi_i)$ of the Dirac's delta distribution has been exploited. Furthermore, in Eqs. (5) and (6), the dimensionless singularity parameters $\gamma_i=\frac{\overline{\gamma}_i}{L}$, and the shear stiffness parameter br^2, with $b=\frac{G_0}{E_0}$ and $r^2=L^2\frac{A_0}{I_0}$, have been introduced.

3. The governing equations for the stability of the Timoshenko beam with multiple cracks

The governing equations of the Timoshenko beam have been formulated in presence of multiple singularities under the form presented in Eqs. (5) and (6). The above mentioned equations are suitably modified in this section, by means of the adoption of the integration rules of the distributions, in order to obtain explicit closed form solutions.

Single integration of Eq. (6) leads to:

$$br^2H(\xi)\left[u^I(\xi)+\varphi(\xi)\right]=-\sigma^2\varphi(\xi)+b_1 \tag{7}$$

where b_1 is an integration constant. Furthermore, substitution of Eq. (7) into Eq. (5), and further integration, provides the following equation:

$$\varphi^I(\xi)=\frac{1}{D(\xi)}\left[\sigma^2u(\xi)+b_1\xi+b_2\right]+\varphi^I(\xi)\sum_{i=1}^{n_\gamma}\gamma_i\delta(\xi-\xi_{\gamma_i}) \tag{8}$$

with b_2 an additional integration constant.

On the other hand, Eq. (7) can be rewritten as follows:

$$u^I(\xi)=\frac{1}{H(\xi)}\left[-\frac{\sigma^2}{br^2}\varphi(\xi)+\frac{b_1}{br^2}\right]-\varphi(\xi) \tag{9}$$

Eq. (8) is a parametric expression of the rotation derivative $\varphi^I(\xi)$ since the summation $\varphi^I(\xi)\sum_{i=1}^{n_\gamma}\gamma_i\delta(\xi-\xi_{\gamma_i})$ appears at the righ-hand side. In order to obtain explicitly the expressions of $\varphi^I(\xi)$ and $u^I(\xi)$ both members of Eq. (8) are multiplied by $\delta(\xi-\xi_{\gamma_k})$ providing the following expression:

$$\varphi^I(\xi)\delta(\xi-\xi_{\gamma_k})=\frac{1}{1-\gamma_kA}\frac{1}{D(\xi)}\left[\sigma^2u(\xi)+b_1\xi+b_2\right]\delta(\xi-\xi_{\gamma_k}) \tag{10}$$

Derivation of Eq. (10) has required the definition of the product of two Dirac's delta distributions providing a single Dirac's delta times a constant A, as already exploited in Biondi and Caddemi

(2005, 2007) where the value $A = 2.013$ (among those proposed by Bagarello (1995, 2002) has been adopted. Substitutions of Eq. (10) into Eq. (8) leads to the following explicit expression of the rotation derivative $\varphi^I(\xi)$ as follows:

$$\varphi^I(\xi) = \frac{1}{D(\xi)}\left[\sigma^2 u(\xi) + b_1\xi + b_2\right]\left[1 + \sum_{i=1}^{n_\gamma}\lambda_{\gamma_i}\delta(\xi - \xi_{\gamma_i})\right] \tag{11}$$

where the dimensionless parameters $\lambda_{\gamma_i} = \frac{\gamma_i}{1 - A\gamma_i}$ have been introduced. The latter quantities λ_{γ_i} will be considered in this work as damage parameters since they can be easily related to the crack depth according to classical crack models as shown in the Appendix.

It must be noted that a different value for the constant A might be adopted, together with the appropriate value of the parameter γ_i, leading to the actual damage parameter value $\lambda_{\gamma_i} = \frac{\gamma_i}{1 - A\gamma_i}$ chosen to provide the equivalence with the crack depth.

In particular, if the case of constant flexural and shear stiffnesses is treated, $D(\xi) = H(\xi) = 1$, Eqs. (11) and (9) are written as follows:

$$\varphi^I(\xi) = \left[\sigma^2 u(\xi) + b_1\xi + b_2\right]\left[1 + \sum_{i=1}^{n_\gamma}\lambda_{\gamma_i}\delta(\xi - \xi_{\gamma_i})\right] \tag{12}$$

$$u^I(\xi) = \frac{b_1}{br^2} - \hat{\sigma}^2\varphi(\xi) \tag{13}$$

where

$$\hat{\sigma}^2 = 1 + \frac{\sigma^2}{br^2} \tag{14}$$

Explicit expressions for the rotation $\varphi(\xi)$ and the normalized deflection $u(\xi)$ functions can be obtained by integration of Eqs. (12) and (13) as outlined in the following section.

The governing equations of the Timoshenko beam in presence of multiple cracks provided by Eqs. (12) and (13) can be, however, reduced to a single equation by means of differentiation of Eq. (13), substitution of Eq. (12), and after simple algebra, providing the following expression for $u^{II}(\xi)$:

$$u^{II}(\xi) + \hat{\sigma}^2\sigma^2 u(\xi) = -\hat{\sigma}^2[b_1\xi + b_2] - \hat{\sigma}^2\sum_{i=1}^{n_\gamma}\left[\sigma^2 u(\xi_{\gamma_i}) + b_1\xi_{\gamma_i} + b_2\right]\lambda_{\gamma_i}\delta(\xi - \xi_{\gamma_i}) \tag{15}$$

If the following positions are introduced:

$$B[u(\xi_{\gamma_i})] = \hat{\sigma}^2[\sigma^2 u(\xi_{\gamma_i}) + b_1\xi_{\gamma_i} + b_2]\lambda_{\gamma_i} \tag{16a}$$

$$\overline{\sigma}^2 = \hat{\sigma}^2\sigma^2 \tag{16b}$$

Eq. (15) can be rewritten as follows:

$$u^{II}(\xi) + \overline{\sigma}^2 u(\xi) = -\hat{\sigma}^2[b_1\xi + b_2] - \sum_{i=1}^{n_\gamma}B[u(\xi_{\gamma_i})]\delta(\xi - \xi_{\gamma_i}) \tag{17}$$

The governing differential equations of the Timoshenko beam in presence of an arbitrary number of cracks and subjected to an axial load, given by Eqs. (5) and (6), have been combined to provide the sole Eq. (17), as function of the deflection $u(\xi)$, whose integration procedure will be presented in the next section.

4. Integration procedure of the governing equation of the Timoshenko beam with multiple cracks

The general solution of Eq. (17) is given by the solution of the corresponding homogeneous equation, $u_h(\xi)$ and a particular integral $u_p(\xi)$ as follows:

$$u(\xi) = u_h(\xi) + u_p(\xi) = \hat{C}_3\sin\overline{\sigma}\xi + \hat{C}_4\cos\overline{\sigma}\xi + u_p(\xi) \tag{18}$$

where $\hat{C}_3, \hat{C}_4$ are integration constants. We seek a particular integral $u_p(\xi)$ under the following form:

$$u_p(\xi) = d_1(\xi)\sin\overline{\sigma}\xi + d_2(\xi)\cos\overline{\sigma}\xi + C_1\xi + C_2 \tag{19}$$

C_1, C_2 being integration constants, and $d_1(\xi)$, $d_2(\xi)$ unknown functions of the normalized variable ξ, to be determined such that Eq. (17) is verified. The first derivative of $u_p(\xi)$ given by Eq. (19) is:

$$u_p'(\xi) = d_1(\xi)\overline{\sigma}\cos\overline{\sigma}\xi - d_2(\xi)\overline{\sigma}\sin\overline{\sigma}\xi + d_1'(\xi)\overline{\sigma}\sin\sigma\xi + d_2'(\xi)\overline{\sigma}\cos\overline{\sigma}\xi + C_1 \tag{20}$$

The search of the particular solution, besides enforcement of the second order governing Eq. (17), will be performed under the following additional condition involving the first derivatives of the functions $d_1(\xi), d_2(\xi)$:

$$d_1'(\xi)\overline{\sigma}\sin\overline{\sigma}\xi + d_2'(\xi)\overline{\sigma}\cos\overline{\sigma}\xi = 0 \tag{21}$$

In view of Eq. (21), the following constrained form for the first derivative $u_p'(\xi)$ of the particular integral can be written:

$$\begin{aligned} &u_p'(\xi) = d_1(\xi)\overline{\sigma}\cos\overline{\sigma}\xi - d_2(\xi)\overline{\sigma}\sin\overline{\sigma}\xi + C_1, \\ &\text{s.t. } d_1'(\xi)\overline{\sigma}\sin\overline{\sigma}\xi + d_2'(\xi)\overline{\sigma}\cos\overline{\sigma}\xi = 0 \end{aligned} \tag{22}$$

in which the derivatives of the unknown functions $d_1(\xi)$ and $d_2(\xi)$ are not involved. In view of Eq. (22) the second derivative $u_p''(\xi)$ of the particular integral may be written as:

$$u_p''(\xi) = -d_1(\xi)\overline{\sigma}^2\sin\overline{\sigma}\xi - d_2(\xi)\overline{\sigma}^2\cos\overline{\sigma}\xi + d_1'(\xi)\overline{\sigma}\cos\overline{\sigma}\xi - d_2'(\xi)\overline{\sigma}\sin\overline{\sigma}\xi \tag{23}$$

Eq. (23), in view of Eq. (19), may be written as follows:

$$u_p''(\xi) = -\overline{\sigma}^2[u_p(\xi) - C_1\xi - C_2] + d_1'(\xi)\overline{\sigma}\cos\overline{\sigma}\xi - d_2'(\xi)\overline{\sigma}\sin\overline{\sigma}\xi \tag{24}$$

By means of substitution of Eq. (24) into the equilibrium Eq. (17), the following expression is obtained:

$$-\overline{\sigma}^2 u_p(\xi) + \overline{\sigma}^2 C_1\xi + \overline{\sigma}^2 C_2 + d_1'(\xi)\overline{\sigma}\cos\overline{\sigma}\xi - d_2'(\xi)\overline{\sigma}\sin\overline{\sigma}\xi + \overline{\sigma}^2 u_p(\xi) = -\hat{\sigma}^2 b_1\xi - \hat{\sigma}^2 b_2 - \sum_{i=1}^{n_\gamma}B[u(\xi_{\gamma_i})]\delta(\xi - \xi_{\gamma_i}) \tag{25}$$

Since $u_p(\xi)$ must satisfy Eq. (25) the following further conditions on constants b_1 and b_2 must be imposed:

$$\begin{aligned} &-\hat{\sigma}^2 b_1 = \overline{\sigma}^2 C_1 \Rightarrow b_1 = -\sigma^2 C_1; \\ &-\hat{\sigma}^2 b_2 = \overline{\sigma}^2 C_2; \Rightarrow b_2 = -\sigma^2 C_2 \end{aligned} \tag{26}$$

Eqs. (21) and (25) represent a first order linear differential set of equations with unknowns functions $d_1(\xi), d_2(\xi)$, that can written as follows:

$$\begin{cases} d_1'(\xi)\overline{\sigma}\sin\overline{\sigma}\xi + d_2'(\xi)\overline{\sigma}\cos\overline{\sigma}\xi = 0 \\ d_1'(\xi)\overline{\sigma}\cos\overline{\sigma}\xi - d_2'(\xi)\overline{\sigma}\sin\overline{\sigma}\xi = -\sum_{i=1}^{n_\gamma}B[u(\xi_{\gamma_i})]\delta(\xi - \xi_{\gamma_i}) \end{cases} \tag{27}$$

where Eq. (26) has been accounted for. Eq. (27) can also be rewritten as follows:

$$\begin{cases} d_1'(\xi) = -\frac{\cos\overline{\sigma}\xi}{\overline{\sigma}}\sum_{i=1}^{n_\gamma}B[u(\xi_{\gamma_i})]\delta(\xi - \xi_{\gamma_i}) \\ d_2'(\xi) = \frac{\sin\overline{\sigma}\xi}{\overline{\sigma}}\sum_{i=1}^{n_\gamma}B_2[u(\xi_{\gamma_i})]\delta(\xi - \xi_{\gamma_i}) \end{cases} \tag{28}$$

Solution of the set of differential Eq. (28) leads to the following expressions for $d_1(\xi), d_2(\xi)$:

$$\begin{cases} d_1(\xi) = -\frac{1}{\overline{\sigma}}\sum_{i=1}^{n_\gamma} B[u(\xi_{\gamma_i})]\cos\overline{\sigma}\xi_{\gamma_i}U(\xi-\xi_{\gamma_i}) + c_1 \\ d_2(\xi) = \frac{1}{\overline{\sigma}}\sum_{i=1}^{n_\gamma} B[u(\xi_{\gamma_i})]\sin\overline{\sigma}\xi_{\gamma_i}U(\xi-\xi_{\gamma_i}), + c_2 \end{cases} \tag{29}$$

c_1, c_2 being integration constants and where $U(\xi-\xi_{\gamma_i})$ are Heaviside's (unit step) distributions ($U(\xi-\xi_{\gamma_i})=0$ for $\xi<\xi_{\gamma_i}$, $U(\xi-\xi_{\gamma_i})=1$ for $\xi>\xi_{\gamma_i}$).

In view of expressions (29) the particular solution expressed by Eq. (19) can be written as follows:

$$u_p(\xi) = -\frac{1}{\overline{\sigma}}\sum_{i=1}^{n_\gamma} B[u(\xi_{\gamma_i})][\cos\overline{\sigma}\xi_{\gamma_i}\sin\overline{\sigma}\xi - \sin\overline{\sigma}\xi_{\gamma_i}\cos\overline{\sigma}\xi]U(\xi-\xi_{\gamma_i}) + c_1\sin\overline{\sigma}\xi + c_2\cos\overline{\sigma}\xi + C_1\xi + C_2 \tag{30}$$

Eq. (30) can also be written as follows:

$$u_p(\xi) = -\frac{1}{\overline{\sigma}}\sum_{i=1}^{n_\gamma} B[u(\xi_{\gamma_i})]\sin\overline{\sigma}(\xi-\xi_{\gamma_i})U(\xi-\xi_{\gamma_i}) + c_1\sin\overline{\sigma}\xi + c_2\cos\overline{\sigma}\xi + C_1\xi + C_2 \tag{31}$$

The general solution of the equilibrium Eq. (17) can be written, in view of Eqs. (18) and (31) as follows:

$$u(\xi) = -\frac{1}{\overline{\sigma}}\sum_{i=1}^{n_\gamma} B[u(\xi_{\gamma_i})]\sin\overline{\sigma}(\xi-\xi_{\gamma_i})U(\xi-\xi_{\gamma_i}) + C_1\xi + C_2 + C_3\sin\overline{\sigma}\xi + C_4\cos\overline{\sigma}\xi \tag{32}$$

where the positions $C_3 = c_1 + \hat{C}_3$, $C_4 = c_2 + \hat{C}_4$ have been introduced.

Substitution of Eq. (16), providing the term $B[u(\xi_{\gamma_i})]$, into Eq. (32) leads to the following expression for the deflection function:

$$u(\xi) = -\sum_{i=1}^{n_\gamma}[\overline{\sigma}u(\xi_{\gamma_i}) - \overline{\sigma}C_1\xi_{\gamma_i} - \overline{\sigma}C_2]\lambda_{\gamma_i}\sin\overline{\sigma}(\xi-\xi_{\gamma_i})U(\xi-\xi_{\gamma_i}) + C_1\xi + C_2, + C_3 sin\ \overline{\sigma}\xi + C_4 cos\ \overline{\sigma}\xi \tag{33}$$

where Eqs. (14) and (26) have been taken into account.

According to Eq. (33) the deflection function $u(\xi)$, at the generic abscissa ξ, depends on the response at the preceding sections, where concentrated cracks occur, in terms of deflection $u(\xi_{\gamma_i})$, $\xi_{\gamma_i}<\xi$. The latter circumstance requires the evaluation of $u(\xi_{\gamma_i})$, for $\xi_{\gamma_i}<\xi$, by making use of the same Eq. (33), which can be rewritten in explicit closed form expression as follows:

$$u(\xi) = C_1 f_1(\xi) + C_2 f_2(\xi) + C_3 f_3(\xi) + C_4 f_4(\xi) \tag{34}$$

The functions $f_j(\xi)$, $j=1,\dots,4$, introduced in Eq. (34), in view of Eq. (33), assume the following expressions:

$$\begin{aligned} f_1(\xi) &= \xi \\ f_2(\xi) &= 1 \\ f_3(\xi) &= \sin\overline{\sigma}\xi - \sum_{i=1}^{n_\gamma}\overline{\sigma}f_3(\xi_{\gamma_i})\lambda_{\gamma_i}\sin\overline{\sigma}(\xi-\xi_{\gamma_i})U(\xi-\xi_{\gamma_i}) \\ f_4(\xi) &= \cos\overline{\sigma}\xi - \sum_{i=1}^{n_\gamma}\overline{\sigma}f_4(\xi_{\gamma_i})\lambda_{\gamma_i}\sin\overline{\sigma}(\xi-\xi_{\gamma_i})U(\xi-\xi_{\gamma_i}) \end{aligned} \tag{35}$$

The first derivative of Eq. (34) gives:

$$u^I(\xi) = C_1 f_1^I(\xi) + C_2 f_2^I(\xi) + C_3 f_3^I(\xi) + C_4\, f_4^I(\xi) \tag{36}$$

where

$$\begin{aligned} f_1^I(\xi) &= 1 \\ f_2^I(\xi) &= 0 \\ f_3^I(\xi) &= \overline{\sigma}\cos\overline{\sigma}\xi - \sum_{i=1}^{n_\gamma}\overline{\sigma}^2 f_3(\xi_{\gamma_i})\lambda_{\gamma_i}\cos\overline{\sigma}(\xi-\xi_{\gamma_i})U(\xi-\xi_{\gamma_i}) \\ f_4^I(\xi) &= -\overline{\sigma}\sin\overline{\sigma}\xi - \sum_{i=1}^{n_\gamma}\overline{\sigma}^2 f_4(\xi_{\gamma_i})\lambda_{\gamma_i}\cos\overline{\sigma}(\xi-\xi_{\gamma_i})U(\xi-\xi_{\gamma_i}) \end{aligned} \tag{37}$$

The second derivative of Eq. (34) gives:

$$u^{II}(\xi) = C_1 f_1^{II}(\xi) + C_2 f_2^{II}(\xi) + C_3 f_3^{II}(\xi) + C_4 f_4^{II}(\xi) \tag{38}$$

in which

$$\begin{aligned} f_1^{II}(\xi) &= 0 \\ f_2^{II}(\xi) &= 0 \\ f_3^{II}(\xi) &= -\overline{\sigma}^2\sin\overline{\sigma}\xi + -\sum_{i=1}^{n_\gamma}\overline{\sigma}^2 f_3(\xi_{\gamma_i})\lambda_{\gamma_i}[-\overline{\sigma}\sin\overline{\sigma}(\xi-\xi_{\gamma_i})U(\xi-\xi_{\gamma_i}) + \cos\overline{\sigma}(\xi-\xi_{\gamma_i})\delta(\xi-\xi_{\gamma_i})] \\ f_4^{II}(\xi) &= -\overline{\sigma}^2\cos\overline{\sigma}\xi + -\sum_{i=1}^{n_\gamma}\overline{\sigma}^2 f_4(\xi_{\gamma_i})\lambda_{\gamma_i}[-\overline{\sigma}\sin\overline{\sigma}(\xi-\xi_{\gamma_i})U(\xi-\xi_{\gamma_i}) + \cos\overline{\sigma}(\xi-\xi_{\gamma_i})\delta(\xi-\xi_{\gamma_i})] \end{aligned} \tag{39}$$

The solution in terms of rotation function $\varphi(\xi)$ can be obtained by substituting Eq. (36) into Eq. (13), and accounting for Eq. (26), as follows:

$$\varphi(\xi) = -\frac{1}{\hat{\sigma}^2}\left[C_1 f_1^I(\xi) + C_2 f_2^I(\xi) + C_3 f_3^I(\xi) + C_4 f_4^I(\xi)\right] - \frac{1}{\hat{\sigma}^2}\frac{\sigma^2}{br^2}C_1 \tag{40}$$

or in the following compact form:

$$\varphi(\xi) = C_1 g_1(\xi) + C_2 g_2(\xi) + C_3 g_3(\xi) + C_4 g_4(\xi) \tag{41}$$

where

$$\begin{aligned} g_1(\xi) &= -\frac{1}{\hat{\sigma}^2}\, f_1^I(\xi) - \frac{1}{\hat{\sigma}^2}\frac{\sigma^2}{br^2} = -\frac{1}{\hat{\sigma}^2}\left(1+\frac{\sigma^2}{br^2}\right) = -1 \\ g_2(\xi) &= -\frac{1}{\hat{\sigma}^2}\, f_2^I(\xi) = 0 \\ g_3(\xi) &= -\frac{1}{\hat{\sigma}^2}\, f_3^I(\xi) \\ g_4(\xi) &= -\frac{1}{\hat{\sigma}^2}\, f_4^I(\xi) \end{aligned} \tag{42}$$

Moreover, the first derivative of Eq. (41) leads to:

$$\varphi^I(\xi) = C_1 g_1^I(\xi) + C_2 g_2^I(\xi) + C_3 g_3^I(\xi) + C_4 g_4^I(\xi) \tag{43}$$

where

$$\begin{aligned} g_1^I(\xi) &= -\frac{1}{\hat{\sigma}^2}\, f_1^{II}(\xi) = 0 \\ g_2^I(\xi) &= -\frac{1}{\hat{\sigma}^2}\, f_2^{II}(\xi) = 0 \\ g_3^I(\xi) &= -\frac{1}{\hat{\sigma}^2}\, f_3^{II}(\xi) \\ g_4^I(\xi) &= -\frac{1}{\hat{\sigma}^2}\, f_4^{II}(\xi) \end{aligned} \tag{44}$$

Eqs. (34) and (41) represent the sought closed-form solution of the governing Eq. (17) and will be exploited to evaluate the buckling load of the Timoshenko beam in presence of multiple cracks.

5. The buckling load equation of multi-cracked Timoshenko columns

The buckling load equation can be derived for Timoshenko columns with multiple cracks by simply imposing the standard boundary conditions, including the general case of rotational and translational spring supports. In this section, the closed form solution presented in Eqs. (34)–(44) are adopted to treat the case of simply supported and clamped–clamped Timoshenko columns. The buckling load equations are derived and numerically solved in order to obtain the critical loads of the considered multi-cracked columns and the corresponding modes. The presented buckling load equations are able to capture the behavior in both cases of compression and tension axial loads. The two cases are recovered for positive and negative values of the solutions, respectively.

5.1. Simply supported column

The boundary conditions of the simply supported Timoshenko column are:

$$u(0)=0,\quad \varphi^I(0)=0,\quad u(1)=0,\quad \varphi^I(1)=0 \tag{45}$$

The four integration constants can be obtained, by imposing the conditions in Eq. (45), as follows:

$$\begin{aligned}
&u(0)=0,\quad \varphi^I(0)=0 \Rightarrow C_2=0,\quad C_4=0\\
&u(1)=0 \Rightarrow C_1+C_3\left[\sin\overline{\sigma}-\sum_{i=1}^{n_\gamma}\overline{\sigma}\lambda_{\gamma_i}f_3(\xi_{\gamma_i})\sin\overline{\sigma}(1-\xi_{\gamma_i})\right]=0\\
&\varphi^I(1)=0 \Rightarrow \frac{1}{\hat{\sigma}^2}C_3\left\{\overline{\sigma}^2\sin\overline{\sigma}-\sum_{i=1}^{n_\gamma}\overline{\sigma}^3 f_3(\xi_{\gamma_i})\lambda_{\gamma_i}\sin\overline{\sigma}(1-\xi_{\gamma_i})\right\}=0
\end{aligned} \tag{46}$$

The last of Eq. (46) leads to the following buckling load equation for the simply supported Timoshenko beam in presence of multiple cracks:

$$\sin\overline{\sigma}-\overline{\sigma}\sum_{i=1}^{n_\gamma}f_3(\xi_{\gamma_i})\lambda_{\gamma_i}\sin\overline{\sigma}(1-\xi_{\gamma_i})=0 \tag{47}$$

Once the smallest solution $\overline{\sigma}_{cr}$ of Eq. (47) is obtained, the value of the first critical load $\sigma^2_{cr}=\frac{N_{cr}L^2}{E_0I_0}$ can be inferred by the definition $\overline{\sigma}^2=\left[1+\frac{\sigma^2}{br^2}\right]\sigma^2$, given by Eq. (16b) in view of Eq. (14), as follows:

$$\frac{\sigma^4_{cr}}{br^2}+\sigma^2_{cr}-\overline{\sigma}^2_{cr}=0 \tag{48}$$

Solution of Eq. (48) leads to the following values for the compression (positive value) ${}^{+}\sigma^2_{cr}$ and tension (negative value) ${}^{-}\sigma^2_{cr}$ critical load parameters:

$$\left.\begin{aligned}{}^{+}\sigma^2_{cr}&=\tfrac{{}^{+}N_{cr}L}{E_0I_0}\\ {}^{-}\sigma^2_{cr}&=\tfrac{{}^{-}N_{cr}L}{E_0I_0}\end{aligned}\right\}=\frac{br^2}{2}\left[-1\pm\sqrt{1+\frac{4}{br^2}\overline{\sigma}^2_{cr}}\right] \tag{49}$$

Furthermore, once the tensile ${}^{-}N_{cr}$ and the compressive ${}^{+}N_{cr}$ critical loads have been evaluated, the relevant buckling modes are determined by means of the evaluation of the integration constants by solving Eq. (46) and substituting in Eq. (34).

5.2. Clamped–clamped column

The boundary conditions of the clamped–clamped column are:

$$u(0)=0,\quad \varphi(0)=0,\quad u(1)=0,\quad \varphi(1)=0 \tag{50}$$

The four integration constants can be obtained, by imposing the conditions in Eq. (45), as follows:

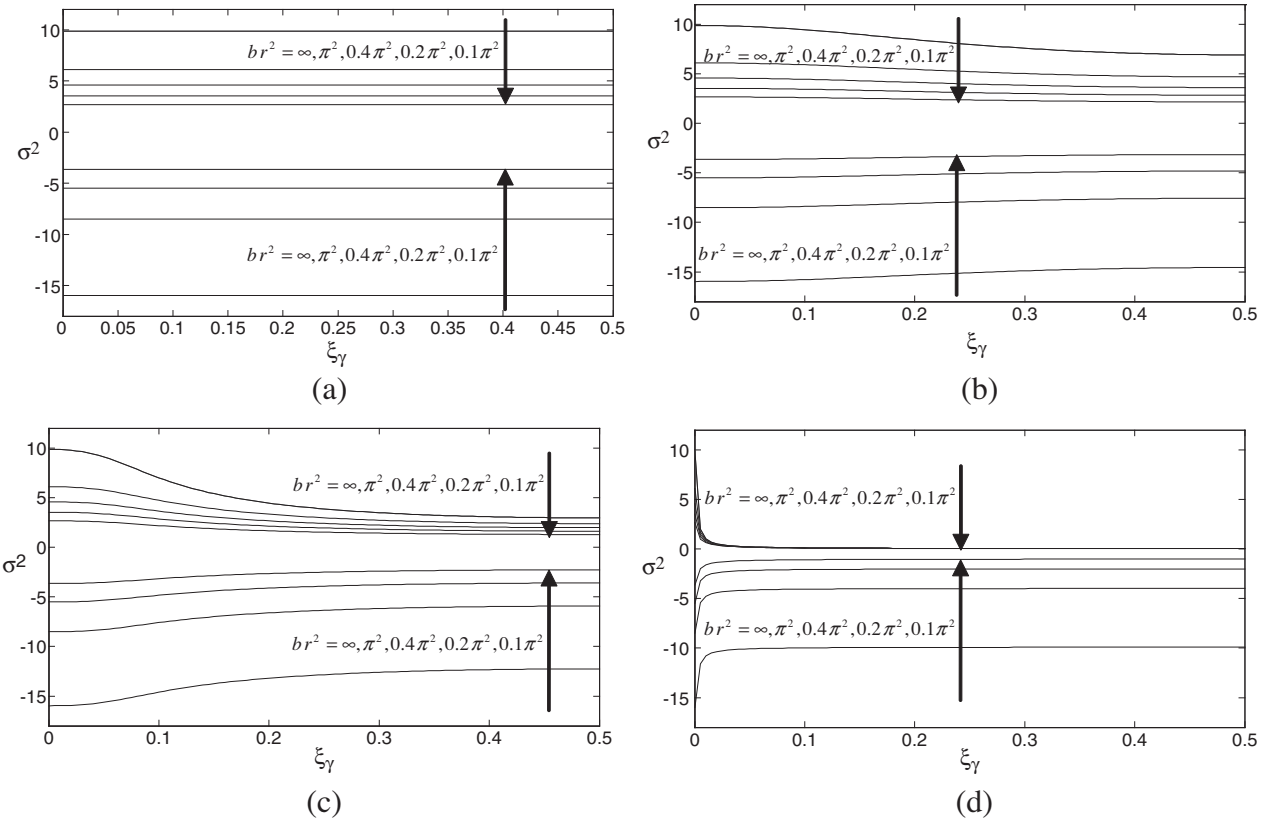

Fig. 1. Critical load parameters ${}^{-}\sigma^2_{cr}$, ${}^{+}\sigma^2_{cr}$ vs crack position ξ_γ for different values of shear stiffness $br^2=\infty,\ \pi^2,\ 0.4\pi^2,\ 0.2\pi^2,\ 0.1\pi^2$ for a simply supported column with a single crack: (a) $\lambda_\gamma=0$; (b) $\lambda_\gamma=0.2$; (c) $\lambda_\gamma=1$; (d) $\lambda_\gamma=100$.

$$
\begin{aligned}
&u(0)=0\Rightarrow C_2=-C_4\\
&\varphi(0)=0\Rightarrow C_1=-C_3\frac{\overline{\sigma}}{\hat{\sigma}^2}\\
&u(1)=0\Rightarrow C_3\left[-\frac{\overline{\sigma}}{\hat{\sigma}^2}+\sin\overline{\sigma}-\sum_{i=1}^{n_\gamma}\overline{\sigma}\lambda_{\gamma_i}f_3(\xi_{\gamma_i})\sin\overline{\sigma}(1-\xi_{\gamma_i})\right]\\
&\qquad+C_4\left[-(1-\cos\overline{\sigma})-\sum_{i=1}^{n_\gamma}\overline{\sigma}\lambda_{\gamma_i}f_4(\xi_{\gamma_i})\sin\overline{\sigma}(1-\xi_{\gamma_i})\right]=0\\
&\varphi(1)=0\Rightarrow C_3\left[(1-\cos\overline{\sigma})+\sum_{i=1}^{n_\gamma}\overline{\sigma}f_3(\xi_{\gamma_i})\lambda_{\gamma_i}\cos\overline{\sigma}(1-\xi_{\gamma_i})\right]\\
&\qquad+C_4\left[\sin\overline{\sigma}+\sum_{i=1}^{n_\gamma}\overline{\sigma}f_4(\xi_{\gamma_i})\lambda_{\gamma_i}\cos\overline{\sigma}(1-\xi_{\gamma_i})\right]=0
\end{aligned}
\tag{51}
$$

Accounting for Eq. (51) leads to the following buckling load equation for the clamped–clamped Timoshenko beam in presence of multiple cracks:

$$
\begin{aligned}
&\left[-\frac{\overline{\sigma}}{\hat{\sigma}^2}+\sin\overline{\sigma}-\sum_{i=1}^{n_\gamma}\overline{\sigma}\lambda_{\gamma_i}f_3(\xi_{\gamma_i})\sin\overline{\sigma}(1-\xi_{\gamma_i})\right]\\
&\times\left[\sin\overline{\sigma}+\sum_{i=1}^{n_\gamma}\overline{\sigma}f_4(\xi_{\gamma_i})\lambda_{\gamma_i}\cos\overline{\sigma}(1-\xi_{\gamma_i})\right]+\\
&-\left[(1-\cos\overline{\sigma})+\sum_{i=1}^{n_\gamma}\overline{\sigma}f_3(\xi_{\gamma_i})\lambda_{\gamma_i}\cos\overline{\sigma}(1-\xi_{\gamma_i})\right]\\
&\times\left[-(1-\cos\overline{\sigma})-\sum_{i=1}^{n_\gamma}\overline{\sigma}\lambda_{\gamma_i}f_4(\xi_{\gamma_i})\sin\overline{\sigma}(1-\xi_{\gamma_i})\right]=0
\end{aligned}
\tag{52}
$$

Differently from the buckling load Eq. (47), for the simply supported case, the parameter $\hat{\sigma}^2$, appears in the buckling load Eq. (52) for the clamped–clamped beam.

In view of Eqs. (14) and (16b) the following relationship between $\hat{\sigma}^2$ and $\overline{\sigma}^2$ holds:

$$
\hat{\sigma}^4-\hat{\sigma}^2-\frac{\overline{\sigma}^2}{br^2}=0 \tag{53}
$$

which can be solved as follows:

$$
\left.\begin{matrix}{}^{+}\hat{\sigma}^2_{cr}\\ {}^{-}\hat{\sigma}^2_{cr}\end{matrix}\right\}==\frac{1\pm\sqrt{1+4\frac{\overline{\sigma}^2}{br^2}}}{2} \tag{54}
$$

From Eq. (54) the expressions of ${}^{+}\hat{\sigma}^2_{cr}$ and ${}^{-}\hat{\sigma}^2_{cr}$ will be adopted for the cases of compression and tension buckling, respectively, to solve the buckling load Eq. (52) in order to provide the smallest solution $\overline{\sigma}_{cr}$.

Once again, the value of the first critical load $\sigma^2_{cr}=\frac{N_{cr}L^2}{E_0I_0}$ can be inferred by means of Eqs. (14) and (16b) as follows:

$$
\left.\begin{matrix}{}^{+}\sigma^2_{cr}=\frac{{}^{+}N_{cr}L}{E_0I_0}\\ {}^{-}\sigma^2_{cr}=\frac{{}^{-}N_{cr}L}{E_0I_0}\end{matrix}\right\}=\frac{br^2}{2}\left[-1\pm\sqrt{1+\frac{4}{br^2}\overline{\sigma}^2_{cr}}\right] \tag{55}
$$

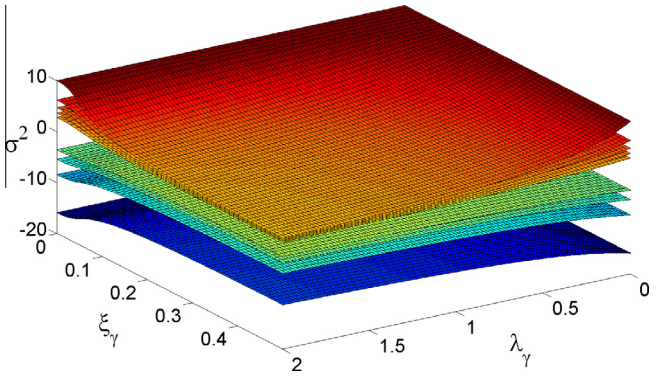

Fig. 2. Critical load parameters ${}^{-}\sigma^2_{cr}$, ${}^{+}\sigma^2_{cr}$ vs crack position ξ_γ and intensity λ_γ for a simply supported column with a single crack for different values of shear stiffness $br^2=\infty,\ \pi^2,\ 0.4\pi^2,\ 0.2\pi^2,\ 0.1\pi^2$.

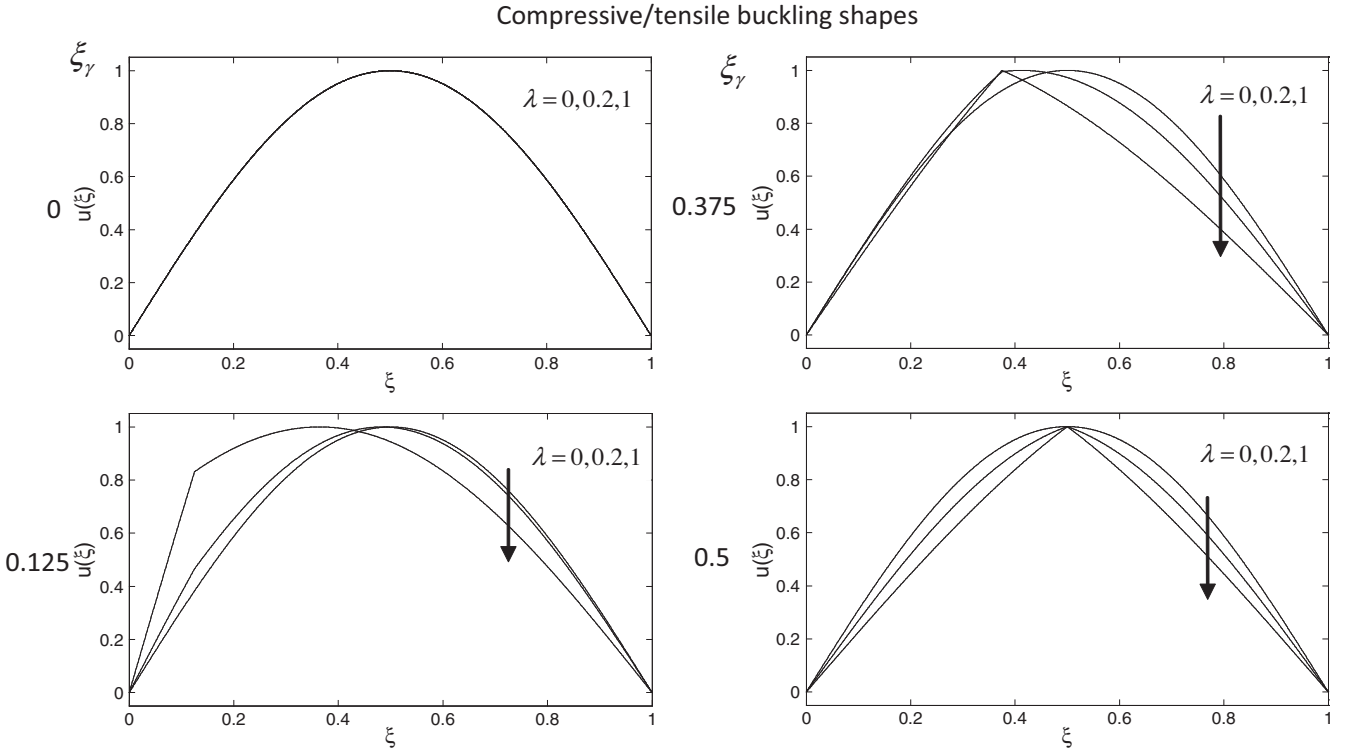

Fig. 3. Compressive/tensile buckling shapes for a simply supported column with a single crack for crack intensity parameter $\lambda_\gamma=0,0.2,1$, for crack position $\xi_\gamma=0,0.125,0.375,0.5$ and for two values of the shear stiffness $br^2=\pi^2$(solid line), $0.1\pi^2$(dashed line).

Fig. 4. A simply supported column with two cracks at symmetric cross-sections.

where ${}^{+}\sigma^2_{cr} = \frac{{}^{+}N_{cr}L}{E_0 I_0}$ and ${}^{-}\sigma^2_{cr} = \frac{{}^{-}N_{cr}L}{E_0 I_0}$ are the compression and tension critical load parameters, respectively.

Finally, once the tensile ${}^{-}N_{cr}$ and the compressive ${}^{+}N_{cr}$ critical loads have been evaluated, the relevant buckling modes are determined by means of the evaluation of the integration constants by solving Eqs. (51) and substituting in Eq. (34).

6. Numerical applications

The presented closed form expressions of the buckling modes and the buckling load equations allow an extensive parametric analysis of columns with multiple cracks by accounting for the influence of the shear deformability.

It has to be remarked that concentrated cracks imply a distributed reduction of the beam stiffness in the vicinity of the damaged section (Christides and Barr, 1984; Sinha et al., 2002; Chondros et al., 1998; Liebowitz et al., 1967; Liebowitz and Claus, 1968; Okamura et al., 1969; Bilello, 2001), as a consequence, a lumped flexibility approach, as that adopted in this work, is accurate for slender beams or it has to be adopted in the case of small crack depths if short beams are accounted for.

Significant effect of the shear deformability is encountered in practice in the case of slender beams composed of materials with a significant shear to Young modulus ratio G_0/E_0, otherwise, for short beams. In this section exact numerical results for the adopted crack model, obtained by means of the presented closed-form solutions, are presented in order to show that tensile buckling loads are comparable with those related to the classical compressive buckling phenomenon. Furthermore, it is shown how the influence of multiple cracks, together with the shear deformability, plays a significant role in this aspect. The presented formulation comprises, as particular case, the results concerning columns with a single crack already available in the literature, and the relevant results are recovered.

An extensive parametric analysis has been conducted by plotting graphs of the buckling load parameter σ^2 and the buckling shapes for different number, position and intensity of the cracks

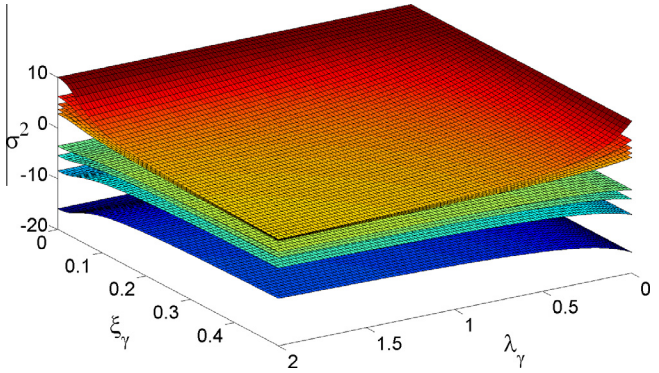

Fig. 6. Critical load parameters ${}^{-}\sigma^2_{cr}$, ${}^{+}\sigma^2_{cr}$ vs crack position ξ_γ and intensity λ_γ for the simply supported column with two cracks in Fig. 4 for different values of shear stiffness $br^2 = \infty,\ \pi^2,\ 0.4\pi^2,\ 0.2\pi^2,\ 0.1\pi^2$.

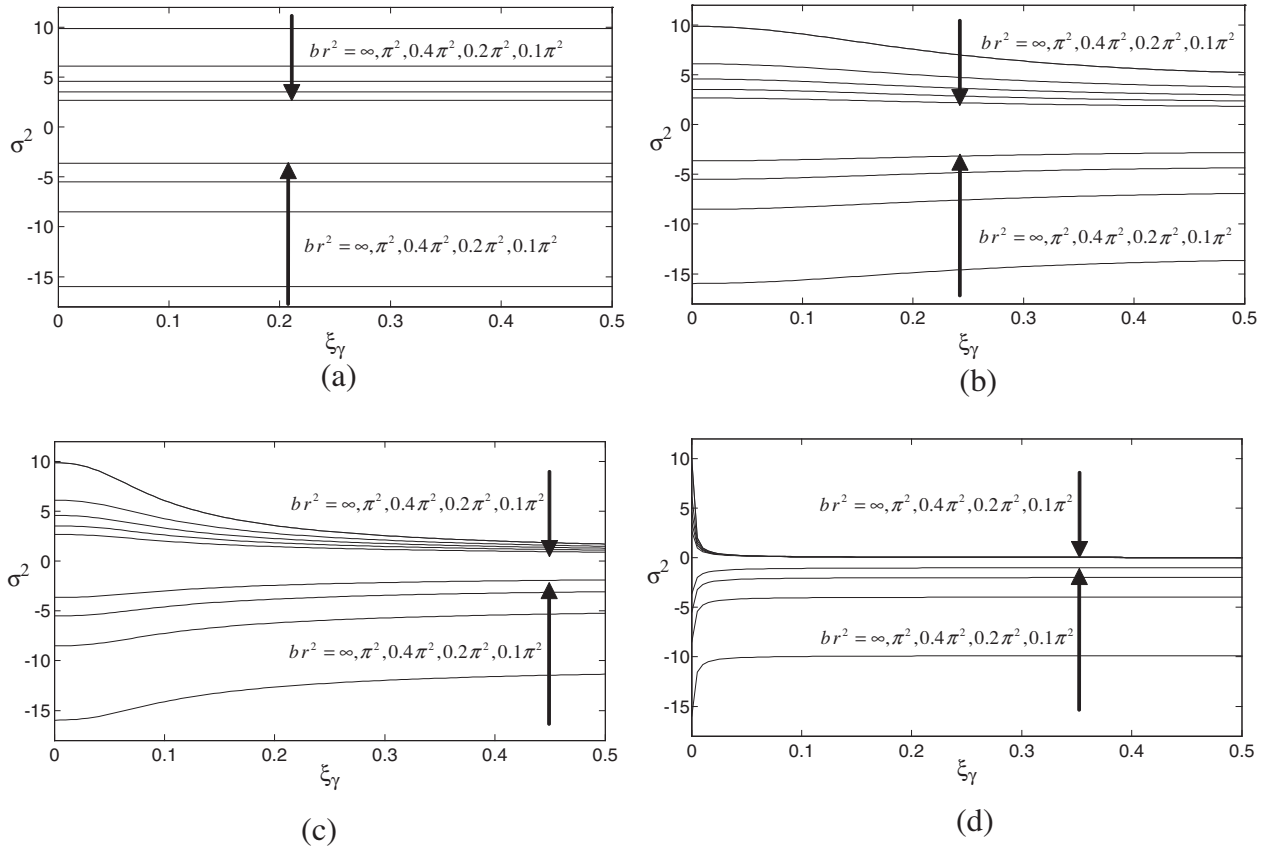

Fig. 5. Critical load parameters ${}^{-}\sigma^2_{cr}$, ${}^{+}\sigma^2_{cr}$ vs crack position ξ_γ for different values of shear stiffness $br^2 = \infty,\ \pi^2,\ 0.4\pi^2,\ 0.2\pi^2,\ 0.1\pi^2$ for the simply supported column with two cracks in Fig. 4: (a) $\lambda_\gamma = 0$; (b) $\lambda_\gamma = 0.2$; (c) $\lambda_\gamma = 1$; (d) $\lambda_\gamma = 100$.

and analyzing the sensitivity with regard to the shear deformability of the column.

The cases of simply supported and clamped–clamped boundary conditions are reported. It is shown how the tensile buckling load is very sensitive to the shear deformability in comparison to the compressive case. Moreover, it is shown how, in the buckling phenomenon due to compressive load, the clamped–clamped beam undergoes abrupt changes of buckling modes from symmetric to anti-symmetric shapes, ruled by the values of the shear deformability with respect to the number, position and intensity of the cracks. A similar behavior has been encountered also in the tensile buckling, where an abrupt change of buckling modes from anti-symmetric to symmetric shapes occurs.

6.1. Simply supported column

The case of simply supported column has been studied by solving Eq. (47) with respect to $\overline{\sigma}$ and evaluating the tensile ${}^{-}\sigma^2_{cr}$ and the compressive ${}^{+}\sigma^2_{cr}$ buckling load parameters by means of Eq. (49). The relevant buckling shapes are given by Eqs. (34) and (41), for the deflection and the rotation functions, respectively, once the integration constants are evaluated by solving the set of Eq. (46).

The buckling behavior of a simply supported column with a single crack is analyzed in Fig. 1 where the critical load parameter vs the crack position along the column axis is plotted for different values of the shear deformability and the crack intensity. The graphs

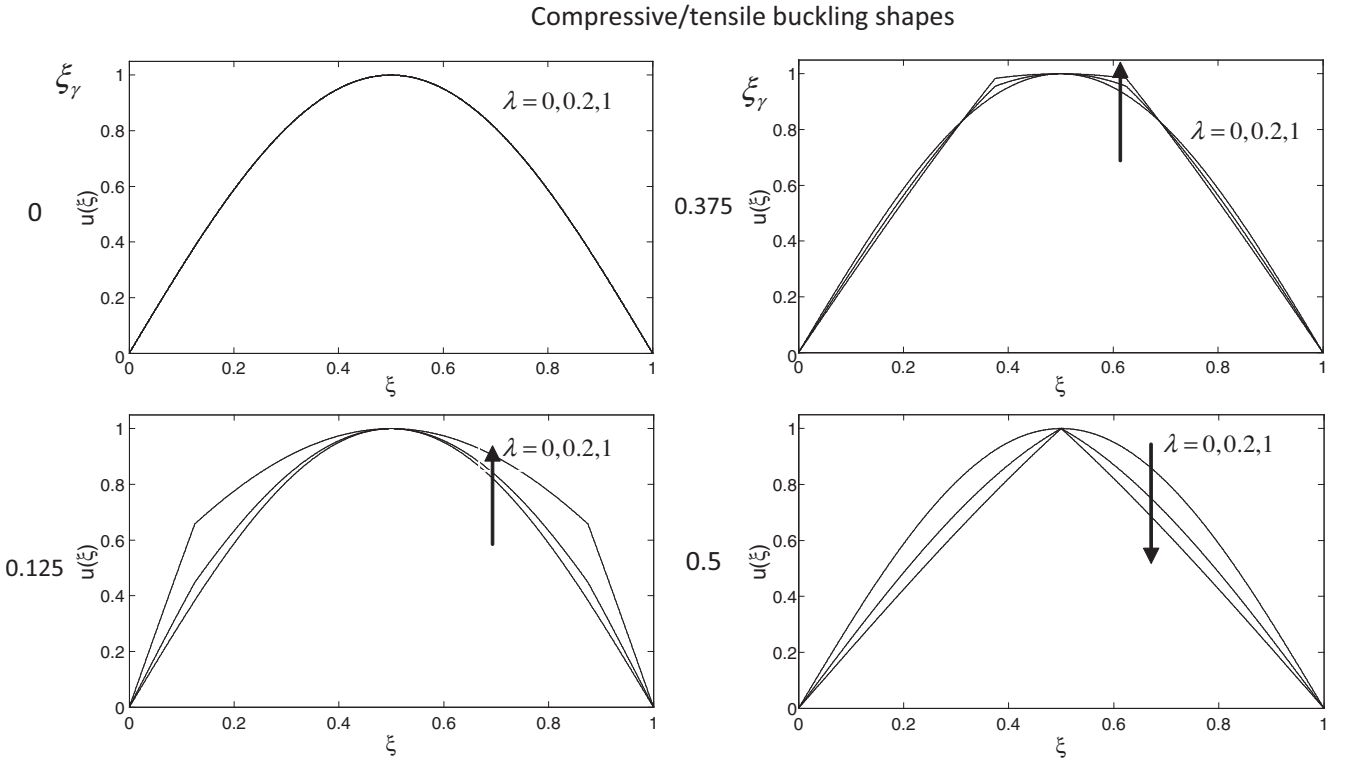

Fig. 7. Compressive/tensile buckling shapes for the simply supported column with two cracks in Fig. 4 for crack intensity parameter $\lambda_\gamma = 0, 0.2, 1$, for crack position $\xi_\gamma = 0, 0.125, 0.375, 0.5$ and for two values of the shear stiffness $br^2 = \pi^2$(solid line), $0.1\pi^2$(dashed line) .

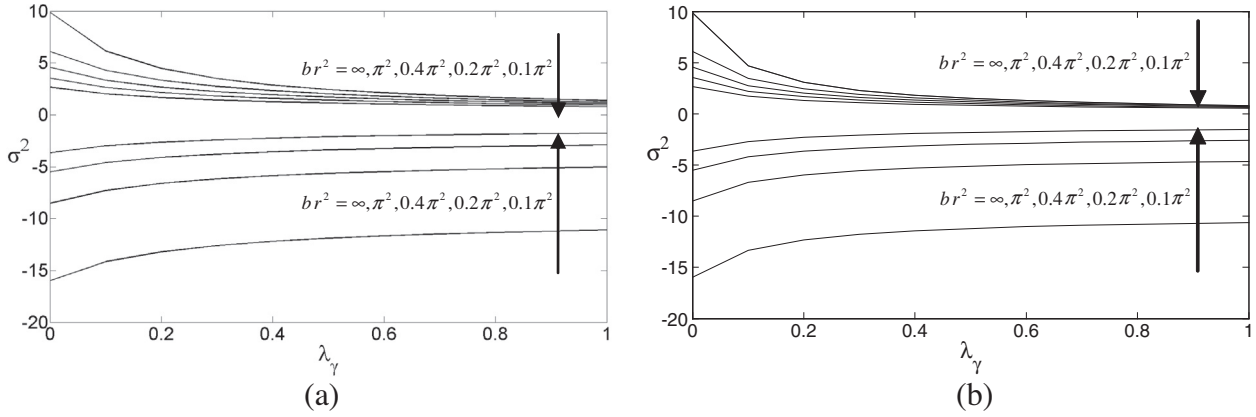

Fig. 8. Critical load parameters ${}^{-}\sigma^2_{cr}$, ${}^{+}\sigma^2_{cr}$ vs the crack intensity parameter λ_γ for a simply supported column with multiple n_γ cracks, uniformly spaced along the span, for different values of shear stiffness $br^2 = \infty,\ \pi^2,\ 0.4\pi^2,\ 0.2\pi^2,\ 0.1\pi^2$: (a) $n_\gamma = 5$; (b) $n_\gamma = 10$.

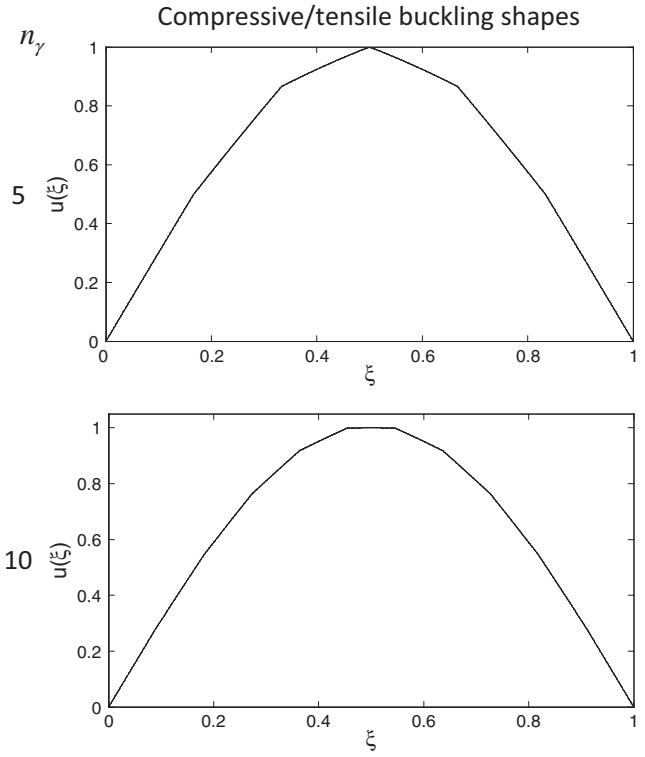

Fig. 9. Compressive/tensile buckling shapes for a simply supported column with multiple $n_\gamma = 5, 10$ cracks, uniformly spaced along the span, for crack intensity parameter $\lambda_\gamma = 1$ and for values of the shear stiffness $br^2 = \pi^2$ (solid line), $0.1\pi^2$ (dashed line).

in Fig. 1 reproduce the results known in the literature for this specific case and confirm that the proposed formulation is consistent with that proposed in Zapata-Medina et al. (2010). Precisely, the buckling load parameter σ^2 adopted in this work is related to P_{cr}/P^* adopted in the latter work as follows $\sigma^2 = \pi^2 P_{cr}/P^*$. As expected, the buckling load values decrease as the crack moves from the left end towards the middle cross-section; the latter attenuation becomes a rapid reduction for the case of high damage intensity $\lambda_\gamma = 100$.

The relationship between the parameter λ_γ with the corresponding geometry and length of the crack is explained in the Appendix. As an example, the extent of the crack associated with the value of λ_γ can be easily inferred by Fig. A2 for the case of a rectangular cross section treated in the Appendix.

The latter results are summarized in the compact form shown in Fig. 2 where the surfaces representing the tensile ${}^{-}\sigma^2_{cr}$ and the compressive ${}^{+}\sigma^2_{cr}$ buckling load parameters vs the crack position and the crack intensity parameter are reported for different values of the shear stiffness. The surfaces reported in Fig. 2 show that the shear deformability has a more pronounced influence on the tensile rather than the compressive buckling load.

In order to show the conditions for physical occurrence of the tensile buckling phenomenon, it has to be noted that it does not appear for extremely high values of the shear stiffness, in fact, elevated values of the tensile buckling load imply that traction failure occurs before the beam buckles. On the other hand, as the shear stiffness decreases the tensile buckling occurs at critical load values comparable to compressive critical load values.

The relevant buckling shapes for the single cracked simply supported column are plotted in Fig. 3 and coincide for the tensile and the compressive buckling. In particular, the buckling shape for crack positions $\xi_\gamma = 0, 0.125, 0.375, 0.5$ and for values of the crack intensity parameters $\lambda_\gamma = 0, 0.2, 1$ are reported. Two values

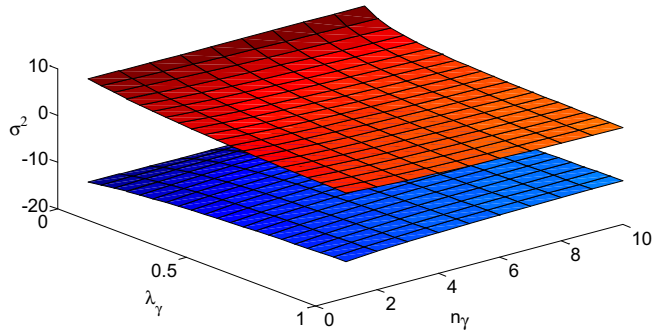

Fig. 10. Critical load parameters ${}^{-}\sigma^2_{cr}$, ${}^{+}\sigma^2_{cr}$ vs the intensity λ_γ and the number n_γ of cracks, uniformly spaced along the span, for the simply supported column for the shear stiffness $br^2 = \pi^2$.

$br^2 = \pi^2, 0.1\pi^2$ have been considered and it can be concluded that the shear stiffness does not have any impact on the buckling shape for the case of single cracked simply supported column.

Moreover the extension presented in this work has been implemented for the case of the simply supported column with two cracks occurring at symmetric cross-sections, as depicted in Fig. 4. Again the results are plotted in Fig. 5 where the critical load parameters vs the crack position ξ_γ along the column axis is plotted for different values of the shear stiffness and the crack intensity. The results for the simply supported column with two cracks are reported in compact form in Fig. 6 where the surfaces representing the tensile ${}^{-}\sigma^2_{cr}$ and the compressive ${}^{+}\sigma^2_{cr}$ buckling load parameters vs the crack position and the crack intensity parameter are reported for different values of the shear stiffness. The buckling shapes for the case of double cracked simply supported column are reported in Fig. 7.

The novelty of the proposed procedure with respect to the others, available in the literature, lies in the capability of capturing the effect of the presence of multiple cracks by means of closed form solutions able to obtain also results concerning the tensile buckling phenomenon. No additional computational cost with respect to the classical undamaged case is required. Hence, finally, since to date extensive analyzes for cases with multiple cracks are not available in the literature, in Figs. 8–10 the case of simply supported column with an increasing number of cracks has been treated. In particular, in Figs. 8 and 9 results in terms of buckling load and shapes, respectively, for $n_\gamma = 5, 10$ cracks are reported. While in Fig. 10 the surfaces representing the tensile ${}^{-}\sigma^2_{cr}$ and the compressive ${}^{+}\sigma^2_{cr}$ buckling load parameters vs the crack intensity parameter λ_γ and the number n_γ of the cracks, uniformly spaced along the span, are reported.

6.2. Clamped–clamped column

In this work, among different boundary conditions acting on shear deformable columns, the clamped–clamped case has been treated since abrupt changes from anti-symmetric to symmetric buckling modes (or vice versa), dependent on the number, position and intensity of the cracks together with the column shear stiffness, have been encountered and are highlighted in this section.

For the clamped–clamped column the tensile ${}^{-}\sigma^2_{cr}$ and the compressive ${}^{+}\sigma^2_{cr}$ buckling load parameters are obtained by solving Eqs. (52)–(55), while the relevant buckling shapes are given by Eqs. (34) and (41), for the deflection and the rotation functions, respectively, once the integration constants are evaluated by solving the set of Eq. (51).

A clamped–clamped column with a single crack has been considered first in order to validate the results obtained with the pro-

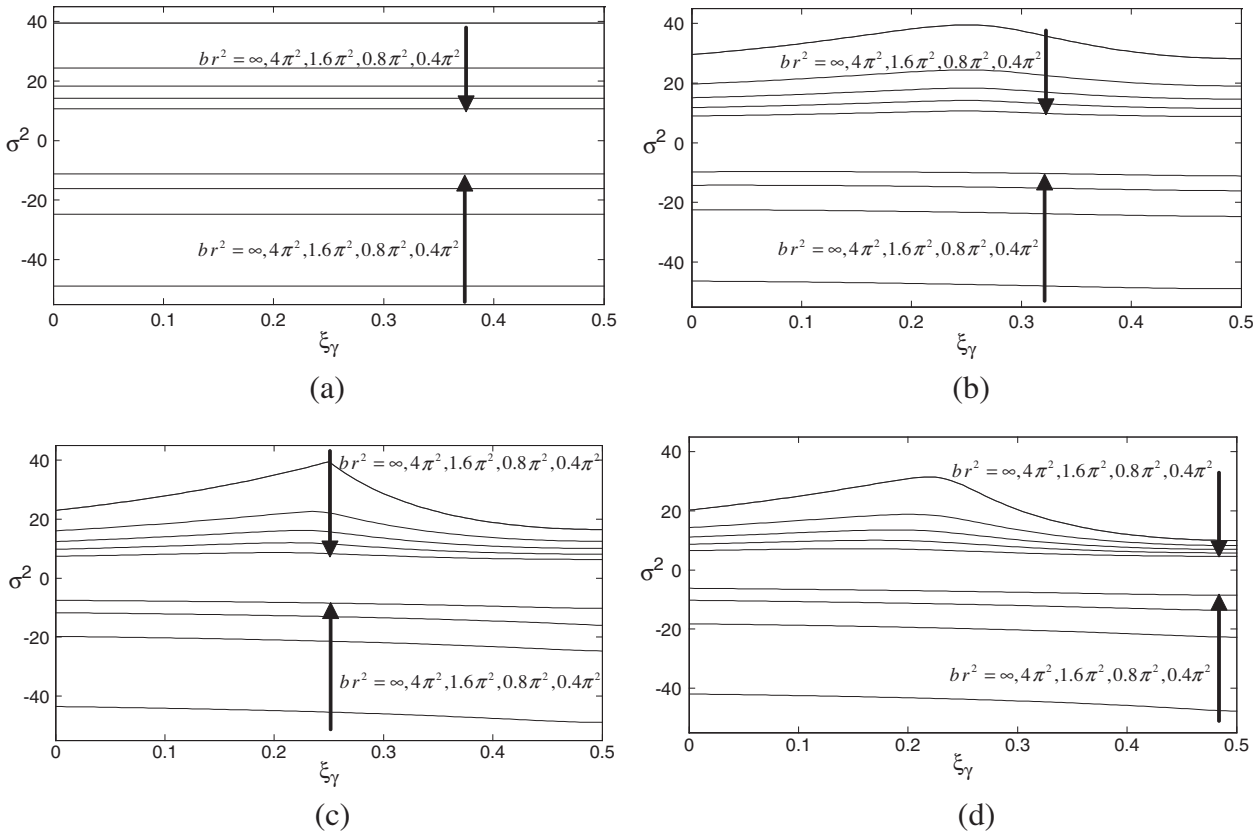

Fig. 11. Critical load parameters ${}^{-}\sigma^2_{cr}$, ${}^{+}\sigma^2_{cr}$ vs crack position ξ_γ for different values of shear stiffness $br^2 = \infty,\ 4\pi^2,\ 1.6\pi^2,\ 0.8\pi^2,\ 0.4\pi^2$ for a clamped–clamped column with a single crack: (a) $\lambda_\gamma = 0$; (b) $\lambda_\gamma = 0.2$; (c) $\lambda_\gamma = 1$; (d) $\lambda_\gamma = 100$.

posed procedure against those available in the literature. In Fig. 11 the critical load parameter vs the crack position is plotted for different values of the shear stiffness and the crack intensity. As already verified for the simply supported column, the results of the particular case of a single crack, also treated in Zapata-Medina et al. (2010), are recovered in Fig. 11. For the classical Euler column, when the crack moves from the left end (i.e. $0 \leqslant \xi_\gamma < 0.25$) the compressive buckling load increases up to its maximum value at $\xi_\gamma = 0.25$ (the inflection point of the undamaged buckling mode), then it decreases as the crack moves towards the middle cross-section (i.e. $0.25 < \xi_\gamma \leqslant 0.5$). Furthermore, when the shear deformation is taken into account, two more comments can be added: (i) accounting for the influence of the shear deformation leads to a reduction of the compressive buckling load; (ii) The position corresponding to the maximum buckling load undergoes a slight drift toward the clamped end.

On the contrary, with regard to the tensile buckling, Fig. 11 shows that the crack position has a very mild influence on the buckling load value even for high crack intensities.

To provide a wider perspective, the results in the case of a single crack are also shown as in Fig. 12 where the surfaces representing the tensile ${}^{-}\sigma^2_{cr}$ and the compressive ${}^{+}\sigma^2_{cr}$ buckling load parameters vs the crack position and the crack intensity parameter are reported for different values of the shear stiffness. The surfaces reported in Fig. 12 show, as the case of simply supported column, that the shear deformability has a moderate impact on the compressive buckling load while it affects considerably the tensile buckling load.

The relevant tensile and compressive buckling shapes for the single cracked clamped–clamped column are plotted in Fig. 13 for crack positions $\xi_\gamma = 0, 0.125, 0.375, 0.5$ and for values of the crack intensity parameters $\lambda_\gamma = 0, 0.2, 1$. The crack position is clearly evidenced by the presence of a kink in the deflection buckling shape. For the compressive buckling shape, the undamaged column undergoes a symmetric deflection shape while some damaged column cases, dependent on the crack position and intensity, are characterized by a change of sign of the deflection shape along the column span. However, the symmetry is preserved only when the middle cross-section is damaged. Two values $br^2 = 4\pi^2, 0.4\pi^2$ have been considered and it can be observed that, unlike the simply supported column, the shear stiffness implies a variation of the buckling shape except when the middle cross-section is cracked. On the other hand, for the undamaged column, the tensile buckling due to the shear deformability leads to an anti-symmetric shape. In the latter case, when a single crack is considered, a kink at the abscissa of the cracked cross-section appears and the deflection buck-

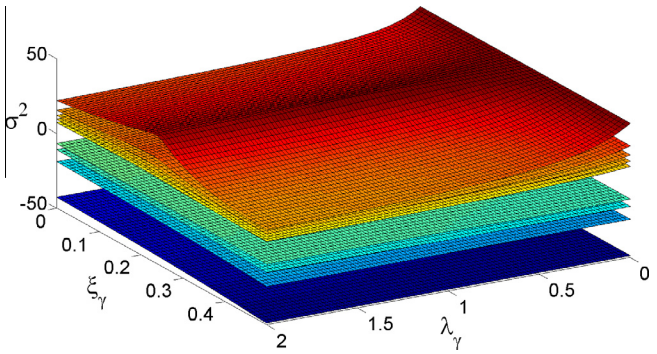

Fig. 12. Critical load parameters ${}^{-}\sigma^2_{cr}$, ${}^{+}\sigma^2_{cr}$ vs crack position ξ_γ and intensity λ_γ for a clamped–clamped column with a single crack for different values of shear stiffness: $br^2 = \infty,\ 4\pi^2,\ 1.6\pi^2,\ 0.8\pi^2,\ 0.4\pi^2$.

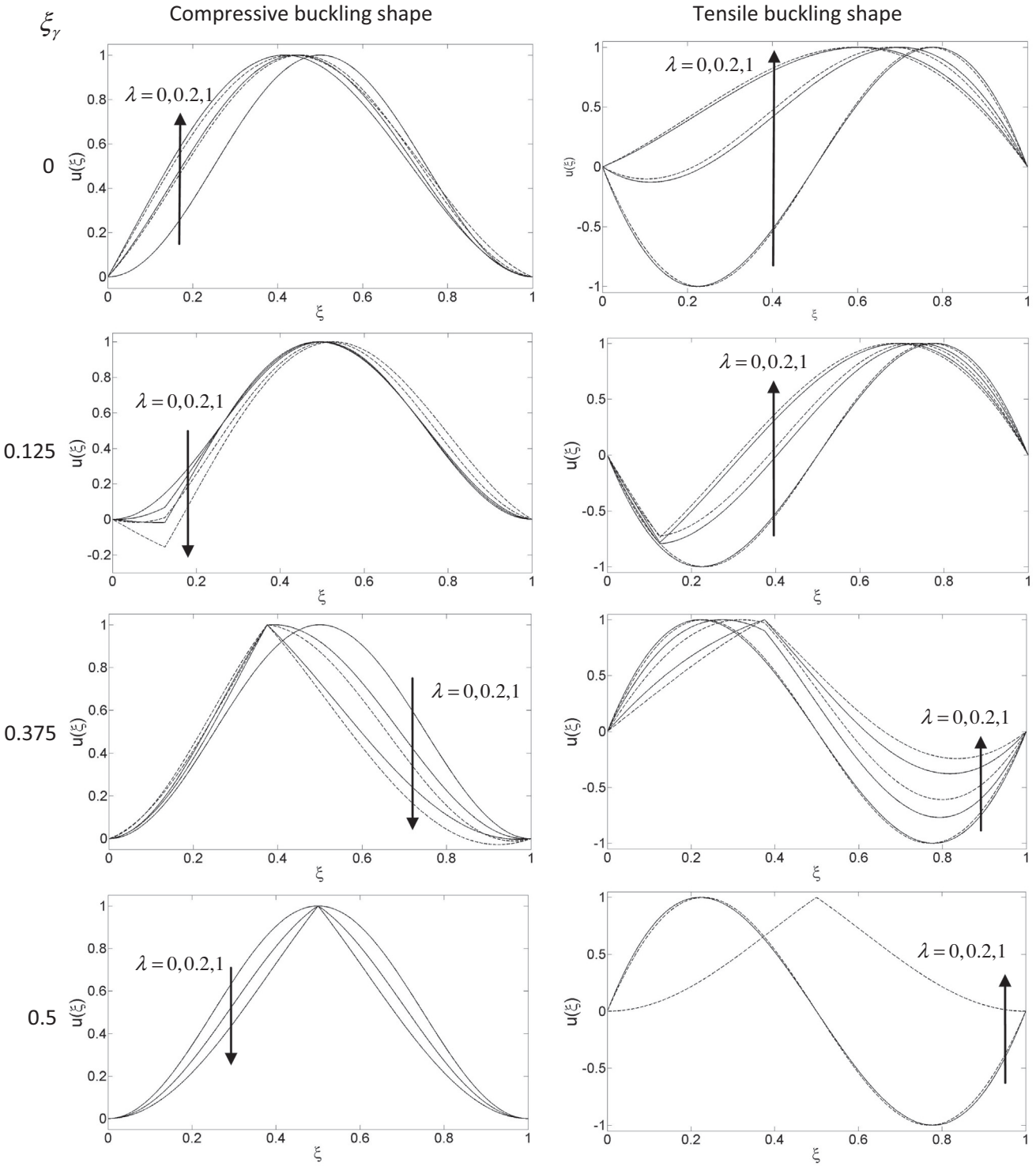

Fig. 13. Compressive (left column) and tensile (right column) buckling shapes for a clamped–clamped column with a single crack for crack intensity parameter $\lambda_\gamma = 0, 0.2, 1$, for crack position $\xi_\gamma = 0, 0.125, 0.375, 0.5$ and for two values of the shear stiffness $br^2 = 4\pi^2$(solid line), $0.4\pi^2$(dashed line).

ling mode drifts from the anti-symmetric shape ($\xi_\gamma = 0, 0.125, 0.375$) and becomes fully symmetric when the crack coincides with the middle cross-section ($\xi_\gamma = 0.5$) for a damage parameter $\lambda_\gamma = 1$ and a low shear stiffness $br^2 = 0.4\pi^2$.

The solutions presented in this work, particularly devoted to multi-cracked columns, have been exploited to analyze the clamped–clamped column with two cracks occurring at symmetric cross-sections in Fig. 14. The critical load parameter vs the distance

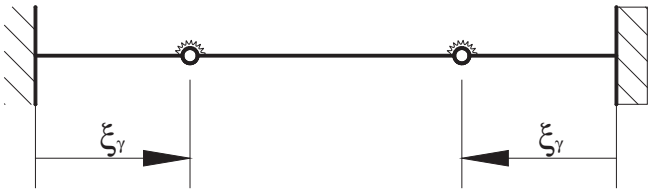

Fig. 14. A clamped–clamped column with two cracks at symmetric cross-sections.

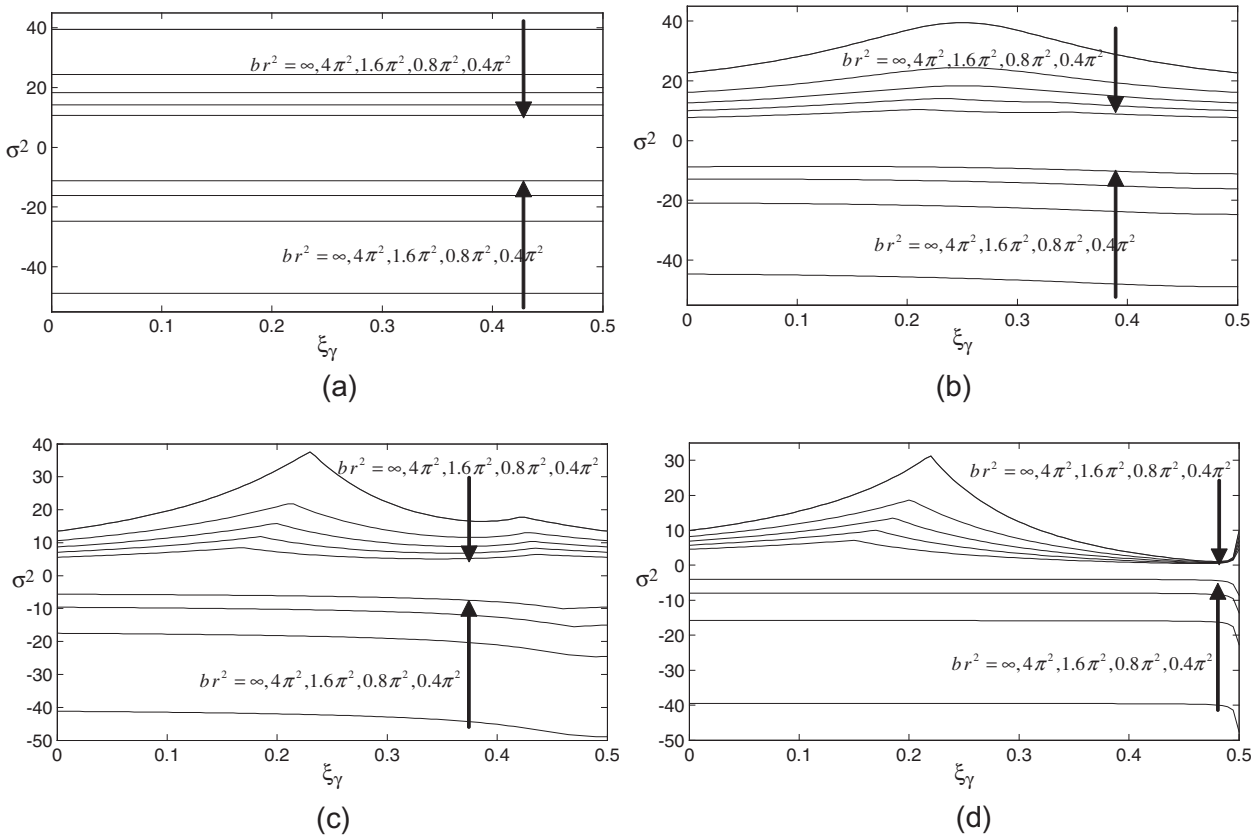

Fig. 15. Critical load parameters ${}^{-}\sigma^2_{cr}$, ${}^{+}\sigma^2_{cr}$ vs crack position ξ_γ for different values of shear stiffness $br^2 = \infty,\ 4\pi^2,\ 1.6\pi^2,\ 0.8\pi^2,\ 0.4\pi^2$ for the clamped-clamped column with two cracks in Fig. 14: (a) $\lambda_\gamma = 0$; (b) $\lambda_\gamma = 0.2$; (c) $\lambda_\gamma = 1$; (d) $\lambda_\gamma = 100$.

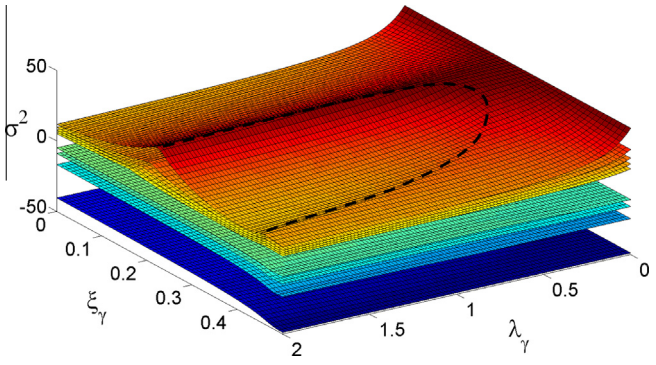

Fig. 16. Critical load parameters ${}^{-}\sigma^2_{cr}$, ${}^{+}\sigma^2_{cr}$ vs crack position ξ_γ and intensity λ_γ for the clamped-clamped column with two cracks in Fig. 14 for different values of shear stiffness $br^2 = \infty,\ 4\pi^2,\ 1.6\pi^2,\ 0.8\pi^2,\ 0.4\pi^2$.

ξ_γ of the cracks from the clamped ends is reported in Fig. 15 for different values of the shear stiffness and the crack intensity ($\lambda_\gamma = 0, 0.2, 1, 100$)). While Fig. 16 shows the complete surfaces of the tensile ${}^{-}\sigma^2_{cr}$ and the compressive ${}^{+}\sigma^2_{cr}$ buckling load parameters vs the crack position and the crack intensity parameter (although in the range $0 \leqslant \lambda_\gamma \leqslant 2$) for different values of the shear stiffness.

The results plotted in Figs. 15 and 16, showing the influence of two cracks on the shear deformable clamped–clamped column, are new and require, for a correct interpretation, a contextual analysis of the relevant buckling modes reported for convenience in Fig. 17.

Precisely, Figs. 15–17 show that, when the two symmetric cracks move closer to each other, the compressive buckling load increases up to its maximum value (at $\xi_\gamma = 0.25$ for infinitely shear rigid columns or at $\xi_\gamma < 0.25$ for shear deformable columns) according to a symmetric buckling mode (compressive buckling shape in Fig. 17 for $\xi_\gamma = 0$ and $\xi_\gamma = 0.125$). Then, the compressive buckling load, on account of the values of the crack intensity and the column shear stiffness with respect to the current crack position, undergoes two alternative different behaviors as the cracks move further towards the middle cross-section (i.e. $0.25 < \xi_\gamma \leqslant 0.5$):

(i) a monotonic reduction (Fig. 15b, for $\lambda_\gamma = 0.2$) with a symmetric mode again (compressive buckling shape in Fig. 17 for $\xi_\gamma = 0.375$ and for $\lambda_\gamma = 0, 0.2$);
(ii) a non-monotonic decrement (Fig. 15c, for $\lambda_\gamma = 1$) with a temporaneous switch to an anti-symmetric mode (compressive buckling shape in Fig. 17 for $\xi_\gamma = 0.375$ and for $\lambda_\gamma = 1$) and the attainment of a successive relative peak indicating the recovery of the simmetric mode (Fig. 17 for compressive buckling with $\xi_\gamma = 0.5$).

The switch to an anti-symmetric mode is clearly indicated by the imprint onto the compression buckling load surface clearly distinguishible for high shear stiffness in Fig. 16. The region outside the imprint is representative of those values of the crack intensity and position leading to symmetric modes.

Furthermore, it has to be noted that, when high values of the crack intensity occur (Fig. 15d, for $\lambda_\gamma = 100$), the decrement due to the occurrence of the anti-symmetric mode reduces the compressive buckling load close to zero and it is followed by a rapid increment as the symmetric shape is recovered.

On the other hand, with regard to the tensile buckling behavior, Figs. 15 and 16 show that as the symmetric cracks move from the clamped ends towards the middle cross-section the tensile buckling load is first subjected to slight increments. Then, at least

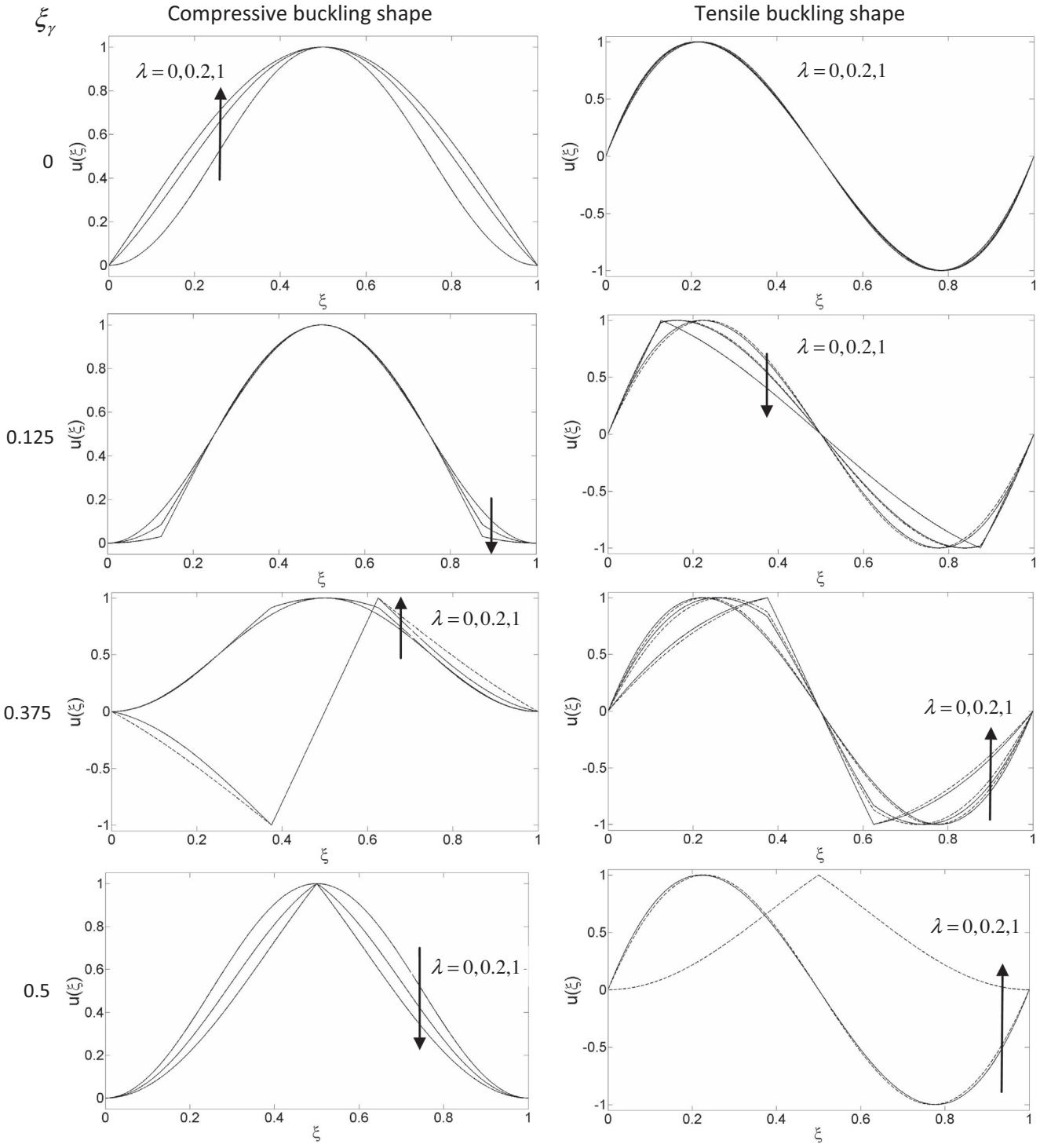

Fig. 17. Compressive (left column) and tensile (right column) buckling shapes for the clamped–clamped column with two cracks in Fig. 14 for crack intensity parameter $\lambda_\gamma = 0, 0.2, 1$, for crack position $\xi_\gamma = 0,\ 0.125,\ 0.375,\ 0.5$ and for two values of the shear stiffness $br^2 = 4\pi^2$(solid line), $0.4\pi^2$(dashed line).

for higher crack intensitites $\lambda_\gamma = 1, 100$ (Fig. 15c,d), as the the two cracks tend to merge at $\xi_\gamma = 0.5$, the tensile buckling load increases suddenly. Moreover, the tensile buckling is characterized by an undamaged anti-symmetric shape that is preserved by the occurrence of two symmetric cracks (Fig. 17 for $\xi_\gamma = 0, 0.125, 0.375$) but is reversed to a symmetric shape when the two cracks are very close to each other (Fig. 17 for $\xi_\gamma = 0.5$) and are characterized by a damage parameter $\lambda_\gamma = 1$ and with low shear stiffness $br^2 = 0.4\pi^2$ of the column.

In addition, both Figs. 15 and 16 show that the tensile buckling load decreases as the column shear stiffness decreases.

The capability of the proposed closed form solutions of capturing the effect of multiple cracks without any additional computational cost with respect to the classical undamaged case has been exploited to analyze the case of clamped–clamped column with an increasing number of cracks. In Figs. 18 and 19 results in terms of buckling load and shapes, respectively, for $n_\gamma = 5, 10$ cracks, uniformly spaced along the span, are reported. In particular, an

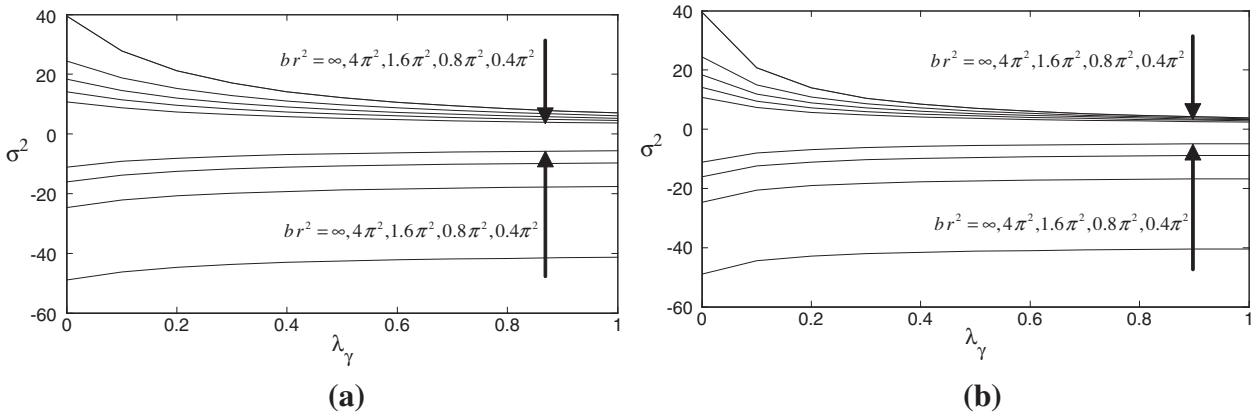

Fig. 18. Critical load parameters $^{-}\sigma^2_{cr}$, $^{+}\sigma^2_{cr}$ vs the crack intensity parameter λ_γ for a clamped–clamped column with multiple n_γ cracks, uniformly spaced along the span, for different values of shear stiffness $br^2 = \infty,\ 4\pi^2,\ 1.6\pi^2,\ 0.8\pi^2,\ 0.4\pi^2$: (a) $n_\gamma = 5$; (b) $n_\gamma = 10$.

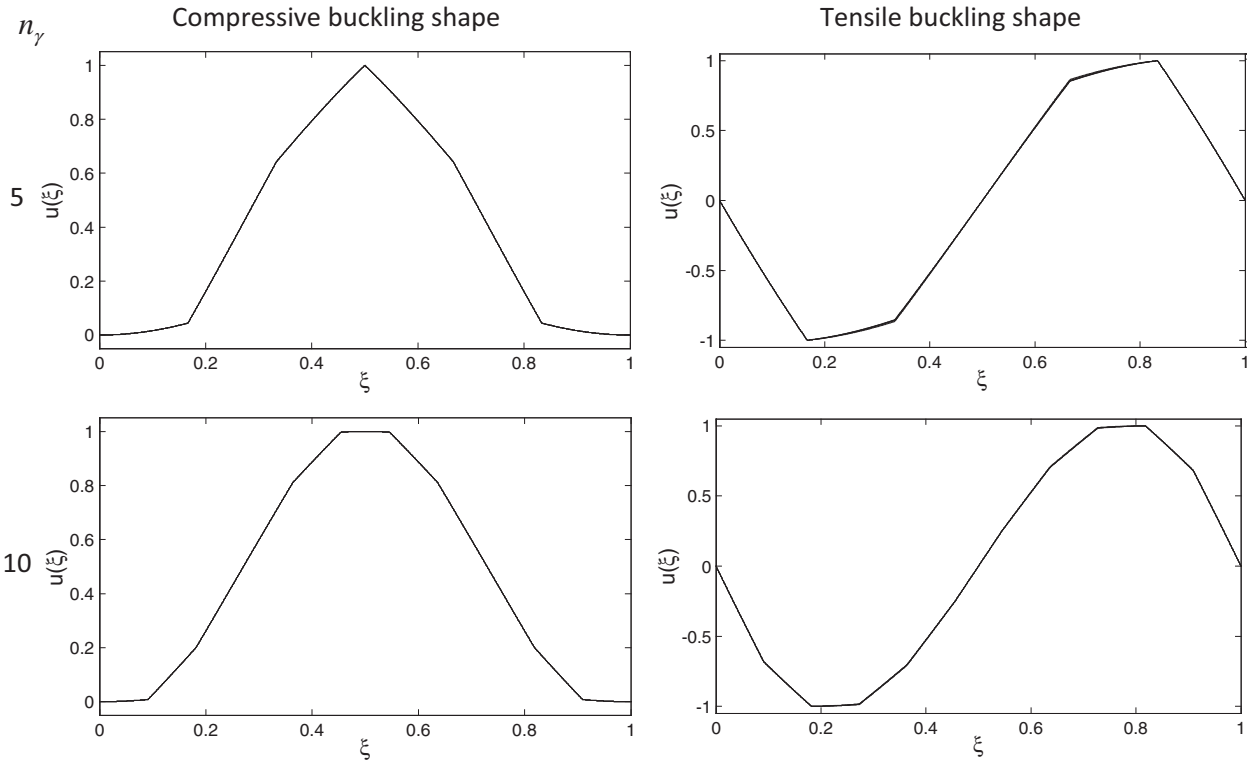

Fig. 19. Compressive (left column) and tensile (right column) buckling shapes for a clamped–clamped column with multiple $n_\gamma = 5, 10$ cracks, uniformly spaced along the span, for crack intensity parameter $\lambda_\gamma = 1$ and for values of the shear stiffness $br^2 = 4\pi^2,\ 0.4\pi^2$.

inspection of Fig. 18 shows that both, compressive and tensile, buckling loads decrease as the crack intensity parameter increases and as the shear stiffness decreases. However, the compressive buckling is always reached with a symmetric shape, while the tensile buckling with an anti-symmetric shape, as depicted in Fig. 19.

A more complete scenario is provided by Fig. 20 where the surfaces representing the tensile $^{-}\sigma^2_{cr}$ and the compressive $^{+}\sigma^2_{cr}$ buckling load parameters vs the crack intensity parameter λ_γ and the number n_γ of the cracks are reported.

Finally, from Fig. 21 the following comment, concerning both cases of simply supported and clamped–clamped multi-cracked columns can be added. Precisely, Figs. 21a and b report the tensile and compressive buckling loads vs the number of cracks, with

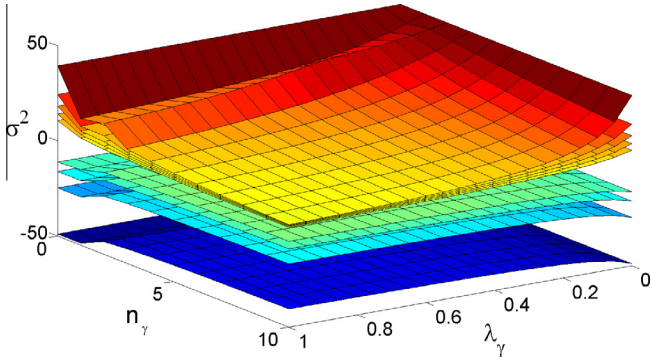

Fig. 20. Critical load parameters $^{-}\sigma^2_{cr}$, $^{+}\sigma^2_{cr}$ vs the intensity λ_γ and the number n_γ of cracks, uniformly spaced along the span, for the clamped–clamped column for different values of shear stiffness: $br^2 = \infty,\ 4\pi^2,\ 1.6\pi^2,\ 0.8\pi^2,\ 0.4\pi^2$.

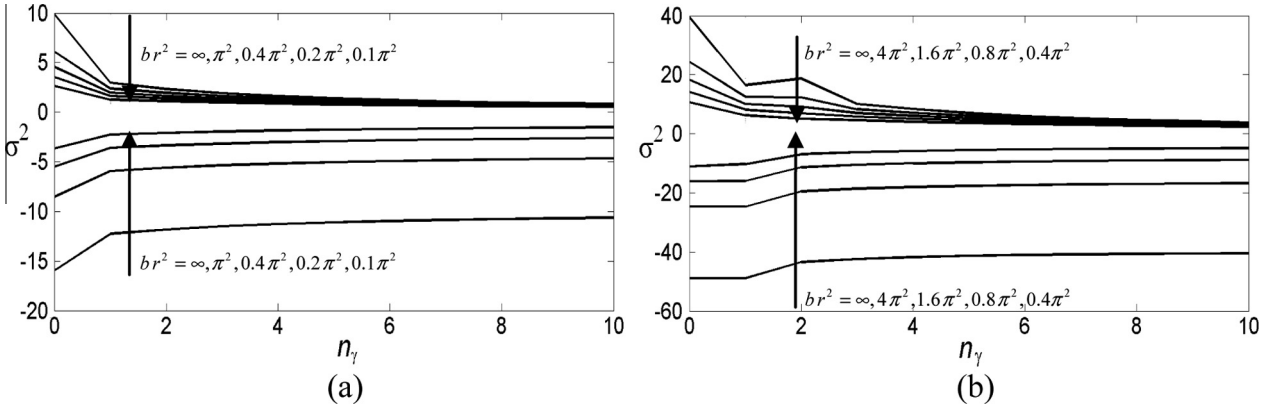

Fig. 21. Critical load parameters ${}^{-}\sigma^2_{cr}$, ${}^{+}\sigma^2_{cr}$ vs the uniformly spaced number of cracks n_γ: (a) pinned-pinned column for $br^2 = \infty,\ \pi^2,\ 0.4\pi^2,\ 0.2\pi^2,\ 0.1\pi^2$; (b) clamped–clamped column for $br^2 = \infty,\ 4\pi^2,\ 1.6\pi^2,\ 0.8\pi^2,\ 0.4\pi^2$.

$\lambda_\gamma = 1$, for different shear stiffness values of the simply supported and the clamped–clamped columns, respectively.

It can be stated that the occurrence of a progressive number of cracks causes a reduction of the compressive buckling load. On the other hand, the tensile buckling load is less sensitive to the occurrence of an increasing number of cracks.

The buckling analysis of beams with multiple cracks has been possible by the presented approach. In particular, the presented closed-form solutions are implemented and provide a direct comparison between compressive and tensile buckling for an increasing number of cracks.

On the other hand, it has been recovered that tensile buckling appears for low values of the shear stiffness parameters. The latter values, particularly those leading to critical load values comparable to the compressive buckling load, can be inferred by the presented figures and adopted to treat the cases of real beams characterized by shear deformable materials.

7. Conclusions

In this work a contribution towards the understanding of the buckling phenomenon of shear deformable damaged columns, in presence of compressive and tensile loads, has been provided. The damage has been considered in the form of multiple cracks modeled as a concentrated flexural stiffness reduction of the column that has been accounted for, in the governing equations, by means of Dirac's delta distributions. An integration procedure leading to closed form solutions of the buckling modes and the buckling load equations has been presented. The proposed explicit solutions concerning the buckling of shear deformable columns, accounting for the presence of an arbitrary number of cracks, represents a novel achievement in the specific literature. Moreover, study of the tensile buckling phenomenon of multi-cracked columns has been possible in this work, for the first time, by means of the proposed explicit solutions. Extensive parametric analyses for multi-cracked simply supported and clamped–clamped columns have been conducted and no additional difficulty with respect to undamaged columns is introduced. The model adopted in this work for the concentrated crack does not account for any influence on the local shear deformability. This latter aspect, however particularly significant in the tensile buckling phenomenon, is not trivial and is currently under investigation.

As future development of the specific case treated in the manuscript, the presented closed form solutions allow the formulation of the explicit closed form stability stiffness matrix of damaged beam elements to treat the case of damaged frames. In the latter case a beam element that makes use of the two extreme nodes only for each damaged element of the frame can be formulated.

Appendix. Relationship between damage parameters and crack depth parameters

In this appendix the damage parameters λ_{γ_i}, adopted in this study to represent concentrated damages and related to the singularity parameters γ_i, appearing in Eq. (2), are shown to be related to the depth of concentrated cracks by making use of the classical crack models provided in the literature.

The rotation function $\varphi(\xi)$, expressed by the closed form solution presented in Eq. (41) shows jump discontinuities $\Delta\varphi(\xi_{\gamma_i})$ at abscissae $\xi_{\gamma_i},\ i = 1,\dots n_\gamma$, that can be expressed as follows:

$$\Delta\varphi(\xi_{\gamma_i}) = \varphi(\xi^+_{\gamma_i}) - \varphi(\xi^-_{\gamma_i}) = \lambda_{\gamma_i}\frac{L}{E_0 I_0}M(\xi_{\gamma_i}), \quad i = 1,\dots,n_\gamma \tag{A1}$$

Where $\xi^+_{\gamma_i}$ and $\xi^-_{\gamma_i}$ are the abscissae at the right and at the left of ξ_{γ_i}, respectively, while $M(\xi_{\gamma_i})$ are the values of the continuous bending moment function at the cracked cross sections, evaluated as $M(\xi_{\gamma_i}) = -EI(\xi_{\gamma_i})u''(\xi_{\gamma_i})/L^2$.

Eq. (A1) provides the relationship between the slope discontinuities $\Delta\varphi(\xi_{\gamma_i})$ and the bending moments $M(\xi_{\gamma_i})$ at ξ_{γ_i}, $i = 1,\dots n_\gamma$ and suggests the interpretation of the adopted flexural stiffness model as internal hinges at ξ_{γ_i} endowed with rotational spring stiffnesses $K^\varphi_{\gamma_i}$ given as:

$$K^\varphi_{\gamma_i} = \frac{E_o I_o}{\lambda_{\gamma_i} L}, \quad i = 1,\dots n_\gamma \tag{A2}$$

Eq. (A2) represents the relationship between $K^\varphi_{\gamma_i}$ and the dimensionless damage parameters λ_{γ_i} related to the singularities introduced in the adopted flexural stiffness model in Eq. (2). It has to be noted that: for $\lambda_{\gamma_i} = 0$, correspondent to the presence of no crack, Eq. (A2) provides $K^\varphi_{\gamma_i} = \infty$; on the other hand, for $\lambda_{\gamma_i} = \infty$, correspondent to an entirely damaged cross-section, Eq. (A2) provides $K^\varphi_{\gamma_i} = 0$.

However, in order to represent the cracks by means of the adopted model a relationship between the damage parameters λ_{γ_i} and the crack depth has to be established.

In the literature various models of concentrated open cracks leading to a continuous description of the beam flexibility in the vicinity of the crack have been proposed (Christides and Barr, 1984; Sinha et al., 2002; Chondros et al., 1998; Liebowitz et al., 1967; Liebowitz and Claus, 1968; Okamura et al., 1969; Bilello 2001). On the other hand, following a macroscopic approach, proposed in the literature, the effect of a concentrated crack can be obtained by means of an equivalent rotational spring with stiffness

K^{eq} placed at the damaged cross-section (Irwin, 1957a,b; Freund and Hermann, 1976). The expressions of the spring stiffness K^{eq} equivalent to the crack are provided for a large number of cases, for different geometry of the cross-section and different crack shapes.

For example, when a lateral crack of uniform depth d is present in a rectangular cross-section of width b and height h, the following expression for the stiffness K^{eq} can be adopted:

$$K^{eq} = \frac{E_0 I_0}{h} \frac{1}{C(\beta)} \tag{A3}$$

where $\beta = d/h$ is defined as the ratio between the crack depth d and the cross-section height h, and $C(\beta)$ is a dimensionless local compliance that can take different forms according to the chosen damage model (Gounaris and Dimarogonas, 1988; Rizos et al., 1990; Ostachowicz and Krawczuk, 1991; Paipetis and Dimarogonas, 1986; Chondros et al., 1998; Bilello, 2001).

The stiffness reduction model proposed by Bilello (2001), for a rectangular cross-section, based on extensive photo-elastic analyses, relies on the presence of an ineffective area around the crack that has approximately a triangular shape. The height of the ineffective area is equal to the crack depth d, while the width $2L_c$ (effective portion of the beam affected by the damage) is given by $d/L_c = 0.9$. The latter expression concerning the effective length L_c was obtained by numerical simulations and confirmed by experimental tests.

The local compliance $C(\beta)$ equivalent to the beam stiffness reduction in the vicinity of the crack can be obtained by imposing that the rotation discontinuity due to the concentrated flexibility reproduces the relative rotation of the cross-sections affected by the crack. For the model proposed by Bilello (2001) the following expression is obtained:

$$C(\beta) = \frac{\beta(2-\beta)}{0.9(\beta-1)^2} \tag{A4}$$

The relationship between the crack model, adopted in this work, and the classical crack models can now be obtained by equating $K^{\varphi}_{\gamma_i}$, given by Eq. (A2), to the rotational spring stiffnesses K^{eq} proposed by the lumped flexibility approach, given by Eq. (A3) and written for the i-th crack, after simple algebra, as follows:

$$\lambda_{\gamma_i} = \frac{h}{L} C(\beta_{\gamma_i}) \tag{A5}$$

Eq. (A5) provides the relationship between the damage parameters λ_{γ_i} and the dimensionless local compliance $C(\beta_{\gamma_i})$, given by the models provided in the literature. Furthermore, according to Eq. (A5), the damage parameters λ_{γ_i} can be given the physical meaning of "dimensionless local compliance", due to the cracks, normalized with respect to the ratio L/h of the beam.

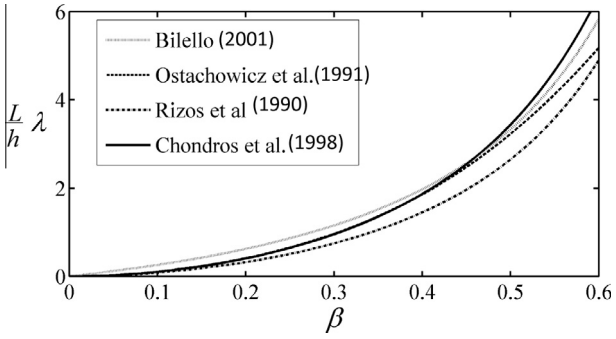

Fig. A1. Damage intensity parameter vs the crack depth to the cross-section height ratio for different models proposed in the literature.

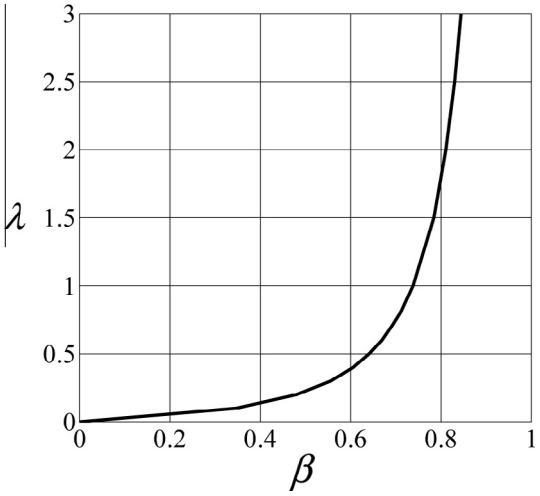

Fig. A2. Damage intensity parameter vs the crack depth to the cross-section height ratio according to the model in (Bilello, 2001) for a beam slenderness $L/h = 15$.

Finally, Eq. (A5) shows that the damage parameters λ_{γ_i} are directly related to the crack depth β_{γ_i}. As a comparison, the quantity $\frac{L}{h}\lambda_{\gamma_i}$ given by Eq. (A5) is plotted in Fig. A1 for some of the expressions of the local compliance $C(\beta_{\gamma_i})$, up to the value $\beta_{\gamma_i} = 0.6$. In addition, in order to provide a specific example, in Fig. A2, the damage parameter λ_{γ_i} against the crack depth β_{γ_i} is reported for the beam slenderness value $L/h = 15$. Fig. A2 shows that a crack with $\lambda_{\gamma_i} = 1$ corresponds to $\beta_{\gamma_i} = 0.737$ that, although it can be considered a severe damage, is not as deep as the depth of the beam. For values of $\beta_{\gamma_i} > 0.8$ the curve in Fig. A2 becomes very steep and the values of λ_{γ_i} increase rapidly. In particular, $\lambda_{\gamma_i} = 100$ (considered in Fig. 1,5,11 and 15) is representative of a crack almost as deep as the depth of the beam (precisely correspondent to $\beta_{\gamma_i} = 0.97$).

References

Anifantis, N., Dimarogonas, A., 1983. Stability of columns with a single crack subjected to follower and vertical loads. International Journal of Solids and Structures 19 (4), 281–291.

Aristizabal-Ochoa, J.D., 2005. Discussion on tension buckling in multilayer elastomeric bearings by James M. Kelly. Journal of Engineering Mechanics ASCE 131, 106–108.

Aristizabal-Ochoa, J.D., 2007. Tension and compression stability and second-order analyses of three dimensional multicolumn systems: effect of shear deformations. Journal of Engineering Mechanics ASCE 133 (1), 106–116.

Bagarello, F., 1995. Multiplication of distribution in one dimension: possible approaches and applications to δ-function and its derivatives. Journal of Mathematical Analysis and Applications 196, 885–901.

Bagarello, F., 2002. Multiplication of distribution in one dimension and a first application to quantum field theory. Journal of Mathematical Analysis and Applications 266, 298–320.

Bilello, C., 2001. Theoretical and experimental investigation on damaged beams under moving systems. Ph.D. Thesis, University of Palermo, Palermo, Italy.

Biondi, B., Caddemi, S., 2005. Closed form solutions of Euler–Bernoulli beams with singularities. International Journal of Solids and Structures 42, 3027–3044.

Biondi, B., Caddemi, S., 2007. Euler–Bernoulli beams with multiple singularities in the flexural stiffness. European Journal of Mechanics A/Solids 26, 789–809.

Buda, G., Caddemi, S., 2007. Identification of concentrated damages in Euler–Bernoulli beams under static loads. Journal of Engineering Mechanics (ASCE) 133 (8), 942–956.

Bueckner, H.F., 1958. The propagation of cracks and the energy of elastic deformation. Transaction of ASME 80, 1225–1229.

Caddemi, S., Caliò, I., 2008. Exact solution of the multi-cracked Euler–Bernoulli column. International Journal of Solids and Structures 45 (16), 1332–1351.

Caddemi, S., Caliò, I., 2009. Exact closed-form solution for the vibration modes of the Euler–Bernoulli beam with multiple open cracks. Journal of Sound and Vibration 327 (3–5), 473–489.

Caddemi, S., Caliò, I., 2012. The influence of the axial force on the vibration of the Euler–Bernoulli beam with an arbitrary number of cracks. Archive of Applied Mechanics 82 (6), 827–839.

Caddemi, S., Caliò, I., 2013a. The exact stability stiffness matrix for the analysis of multi-cracked frame structures. Computers and Structures 125, 137–144.
Caddemi, S., Caliò, I., 2013b. The exact dynamic stiffness matrix of multi-cracked Euler-Bernoulli beam and applications to damaged frame structures. Journal of Sound and Vibrations 332, 3049–3063.
Caddemi, S., Morassi, A., 2013. Multi-cracked Euler–Bernoulli beams: mathematical modeling and exact solutions. International Journal of Solids and Structures 50, 944–956.
Caddemi, S., Caliò, I., Marletta, M., 2010. The non-linear dynamic response of the Euler–Bernoulli beam with an arbitrary number of switching cracks. International Journal of Non-linear Mechanics 45, 714–726.
Caddemi, S., Caliò, I., Cannizzaro, F., 2013. Closed-form solutions for stepped Timoshenko beams with internal singularities and along-axis external supports. Archive of Applied Mechanics 83, 559–577.
Calio, I., Elishakoff, I., 2002. Can harmonic functions constitute closed form buckling modes of inhomogeneous columns. AIAA Journal 40 (12), 2523–2537.
Calio, I., Elishakoff, I., 2004a. Can a trigonometric function serve both as the vibration and the buckling mode of an axially graded structure. Mechanics Based Design of Structures and Machines 32, 401–421.
Calio, I., Elishakoff, I., 2004b. Closed form trigonometric solutions for inhomogeneous beam columns on elastic foundation. International Journal of Structural Stability and Dynamics 4, 139–146.
Calio, I., Elishakoff, I., 2005. Closed form solutions for axially graded beam columns. Journal of Sound and Vibration 280 (1083), 1094.
Challamel, N., Xiang, Y., 2010. On the influence of the unilateral damage behaviour in the stability of cracked beam/columns. Engineering Fracture Mechanics 77, 1467–1478.
Cheng, S.M., Wu, X.J., Wallace, W., 1999. Vibrational response of a beam with a breathing crack. Journal of Sound and Vibration 225, 201–208.
Chondros, T.J., Dimarogonas, A.D., Yao, J., 1998. A continuous cracked beam vibration theory. Journal of Sound and Vibration 215 (1), 17–34.
Christides, S., Barr, A.D.S., 1984. One-dimensional theory of cracked Bernoulli-Euler beams. International Journal of Mechanical Sciences 26 (11/12), 639–648.
Chu, Y.C., Shen, M.H.H., 1992. Analysis of forced bilinear oscillators and the application to cracked beam dynamics. American Institute of Aeronautics and Astronautics 30, 2512–2519.
Dimarogonas, A.D., 1996. Vibration of cracked structures: a state of the art review. Engineering Fracture Mechanics 55, 831–857.
Elishakoff, I., 2005. Eigenvalues of Inhomogenous Structures: Unusual Closed-form Solutions. CRC Press INC.
Falsone, G., 2002. The use of generalised functions in the discontinuous beam bending differential equations. International Journal of Engineering Education 18 (3), 337–343.
Fan, S.C., Zheng, D.Y., 2003. Stability of a cracked Timoshenko beam column by modified Fourier series. Journal of Sound and Vibration 264, 475–484.
Freund, L.B., Hermann, G., 1976. Dynamic fracture of a beam or plate in plane bending. Journal of Applied Mechanics 76, 112–116.
Gounaris, G., Dimarogonas, A.D., 1988. A finite element of a cracked prismatic beam for structural analysis. Computers and Structures 28, 309–313.
Gurel, M.A., 2007. Buckling of slender prismatic circular columns weakened by multiple edge crack. Acta Mechanica 188, 1–19.
Ibrahim, A., Ismail, F., Martin, H.R., 1990. Identification of fatigue cracks from vibration testing. Journal of Sound and Vibration 140, 305–317.
Irwin, G.R., 1957a. Analysis of stresses and strains near the end of a crack traversing a plate. Journal of Applied Mechanics 24, 361–364.
Irwin, G.R., 1957b. Relation of stresses near a crack to the crack extension force. In: 9th Congr. Appl. Mech., Brussels.
Kelly, J.M., 2003. Tension buckling in multilayer elastomeric bearings. Journal of Engineering Mechanics ASCE 129 (12), 1363–1368.
Khiem, N.T., Lien, T.V., 2001. A simplified method for natural frequency analysis of a multiple cracked beam. Journal of Sound and Vibration 245 (4), 737–751.
Li, Q.S., 2001. Buckling of multi-step cracked columns with shear deformation. Engineering Structures 23, 356–364.
Li, Q.S., 2002. Buckling of an elastically restrained multi-step non-uniform beam with multiple cracks. Archive of Applied Mechanics 72, 522–535.
Liebowitz, H., Claus Jr., W.D.S., 1968. Failure of notched columns. Engineering Fracture Mechanics 1, 379–383.
Liebowitz, H., Vanderveldt, H., Harris, D.W., 1967. Carrying capacity of notched column. International Journal of Solids and Structures 3, 489–500.
Okamura, H., Liu, H.W., Chu, C.S., Liebowitz, H., 1969. A cracked column under compression. Engineering Fracture Mechanics 1, pp. 547–564.
Ostachowicz, W.M., Krawczuk, C., 1991. Analysis of the effect of cracks on the natural frequencies of a cantilever beam. Journal of Sound and Vibration 150 (2), 191–201.
Paipetis, S.A., Dimarogonas, A.D., 1986. Analytical Methods in Rotor Dynamics. Elsevier Applied Science, London.
Patel, T.H., Darpe, A.K., 2008. Influence of crack breathing model on nonlinear dynamics of a cracked rotor. Journal of Sound and Vibration 311, 953–972.
Pugno, N., Surace, C., Ruotolo, R., 2000. Evaluation of the non-linear dynamic response to harmonic excitation of a beam with several breathing cracks. Journal of Sound and Vibration 235 (5), 749–762.
Quian, G.L., Gu, S.N., Jiang, J.S., 1990. The dynamic behaviour and crack detection of a beam with a crack. Journal of Sound and Vibration 138, 233–243.
Rizos, P.F., Aspragathos, N., Dimarogonas, A.D., 1990. Identification of crack location and magnitude in a cantilever beam from the vibration modes. Journal of Sound and Vibration 138 (3), 381–388.
Ruotolo, R., Surace, C., 2004. Natural frequencies of a bar with multiple cracks. Journal of Sound and Vibration 272, 301–316.
Shen, M.H.H., Chu, Y.C., 1992. Vibration of beams with a fatigue crack. Computers and Structures 45, 79–93.
Shifrin, E.I., Ruotolo, R., 1999. Natural frequencies of a beam with an arbitrary number of cracks. Journal of Sound and Vibration 222, 409–423.
Sinha, J.K., Friswell, M.I., Edwards, S., 2002. Simplified models for the location of cracks in beam structures using measured vibration data. Journal of Sound and Vibration 251 (1), 13–38.
Sorrentino, S., Fasana, A., Marchesiello, S., 2007. Analysis of non-homogeneous Timoshenko beams with generalized damping distributions. Journal of Sound and Vibration 304 (3–5), 779–792.
Tada, H., Paris, P.C., Irwin, G.R., 1985. The Stress Analysis of Cracks Handbook. Del Research Corporation, Hellertown, Pennsylvania, USA.
Takahashi, I., 1999. Vibration and stability of non-uniform cracked Timoshenko beam subjected to follower force. Computers and Structures 71, 585–591.
Timoshenko, S., Gere, J., 1961. Theory of Elastic Stability. McGraw-Hill, New York.
Vadillo, G., Loya, J.A., Fernandez-Saez, J., 2012. First order solutions for the buckling loads of weakened Timoshenko columns. Computers and Mathematics with Applications 64 (8), 2395–2407.
Wang, Q., 2004. A comprehensive stability analysis of a cracked beam subjected to follower compression. International Journal of Solids and Structures 41, 4875–4888.
Wang, J., Quiao, P., 2007. Vibration of beams with arbitrary discontinuities and boundary conditions. Journal of Sound and Vibration 308, 12–27.
Wang, C.Y., Wang, C.M., Aung, T.M., 2004. Buckling of a weakened column. Journal of Engineering Mechanics ASCE 130, 1373–1376.
Wang, C.M., Wang, C.Y., Reddy, J.N., 2005. Exact Solutions for Buckling of Structural Members. CRC Press INC.
Westmann, R.A., Yang, W.H., 1967. Stress analysis of cracked rectangular beams. Journal of Applied Mechanics 32, 693–701.
Yavari, A., Sarkani, S., 2001. On applications of generalised functions to the analysis of Euler–Bernoulli Beam-columns with jump discontinuities. International Journal of Mechanical Sciences 43, 1543–1562.
Yavari, A., Sarkani, S., Moyer, E.T., 2000. On Applications of generalised functions to beam bending problems. International Journal of Solids and Structures 37, 5675–5705.
Yavari, A., Sarkani, S., Reddy, J.N., 2001a. On nonuniform Euler–Bernoulli and Timoshenko beams with jump discontinuities: application of distribution theory. International Journal of Solids and Structures 38, 8389–8406.
Yavari, A., Sarkani, S., Reddy, J.N., 2001b. Generalised solutions of beams with jump discontinuities on elastic foundations. Archive of Applied Mechanics 71 (9), 625–639.
Zaccaria, D., Bigoni, D., Noselli, G., Misseroni, D., 2011. Structures buckling under tensile dead load. Proceedings of the Royal Society A 467 (2130), 1686–1700.
Zapata-Medina, D.G., Arboleda-Monsalve, L.G., Aristizabal-Ochoa, J.D., 2010. Static stability formulas of a weakened Timoshenko column: effects of shear deformations. Journal of Engineering Mechanics ASCE 136 (12), 1528–1536.
Zastrau, B., 1985. Vibration of cracked structures. Archives of Mechanics 37, 731–743.
Zheng, D.Y., Fan, S.C., 2001a. Natural frequencies of a non-uniform beam with multiple cracks via modified Fourier series. Journal of Sound and Vibration 242, 701–717.
Zheng, D.Y., Fan, S.C., 2001b. Natural frequency changes of a cracked Timoshenko beam by modified Fourier series. Journal of Sound and Vibration 246, 297–317.